WROCŁAW UNIVERSITY OF ENVIRONMENTAL AND LIFE SCIENCES

Contribution of LARES-2 to Space Geodesy

Krzysztof Sośnica, Filip Gałdyn, Joanna Najder, Tomasz Kur, Adrian Nowak, Radosław Zajdel, Dariusz Strugarek

Institute of Geodesy and Geoinformatics, UPWr

Lense-Thirring effect – confirmation using geodetic satellites

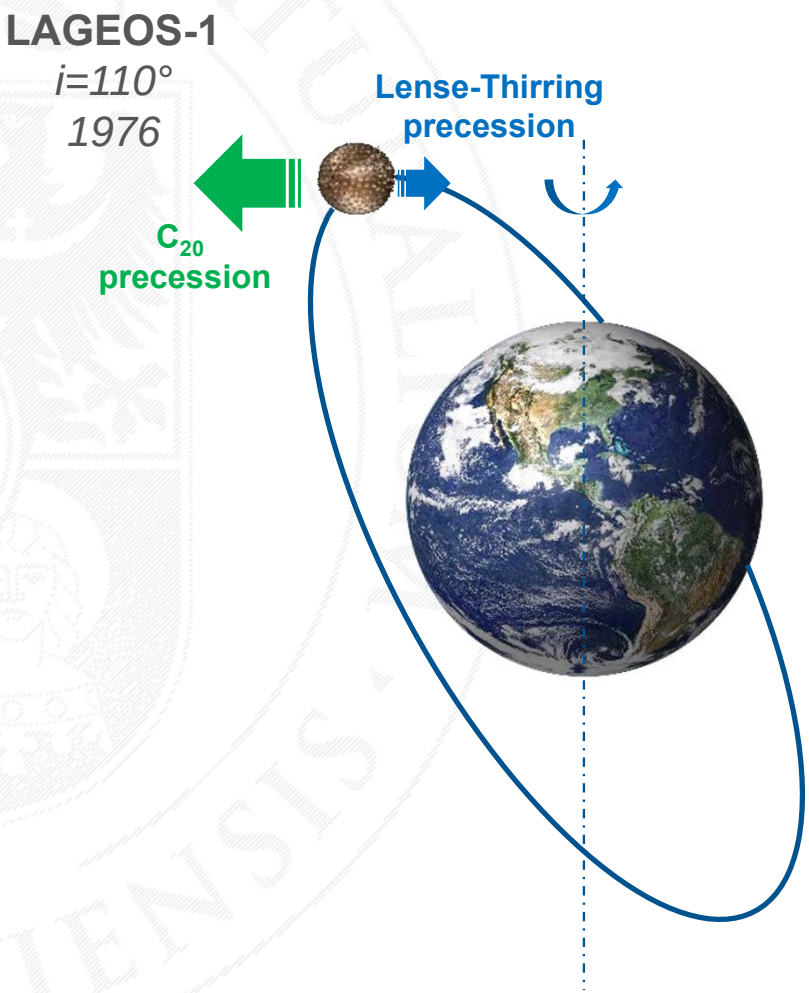

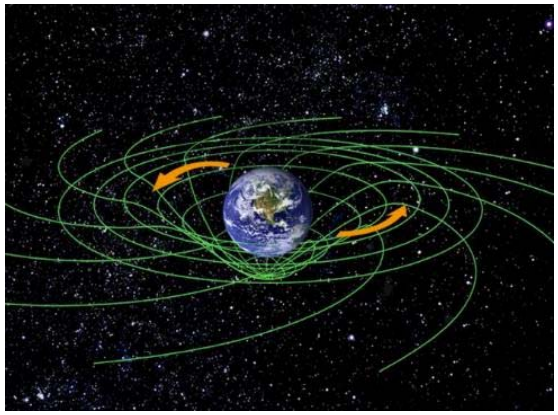

Lense-Thirring

$$\Delta\Omega_{LT} = 2\frac{GM_{\oplus}J_{\oplus}}{c^2a^3(1-e^2)^{\frac{3}{2}}}\Delta t$$

$$\Delta\Omega_{C_{20}} = -\frac{3}{2}\sqrt{\frac{GM_{\oplus}}{r_{\oplus}^3}}\left(\frac{r_{\oplus}}{a}\right)^{\frac{7}{2}}\frac{\cos(i)}{(1-e^2)^2}C_{2,0}\,\Delta t$$

Lense-Thirring effect – confirmation using geodetic satellites

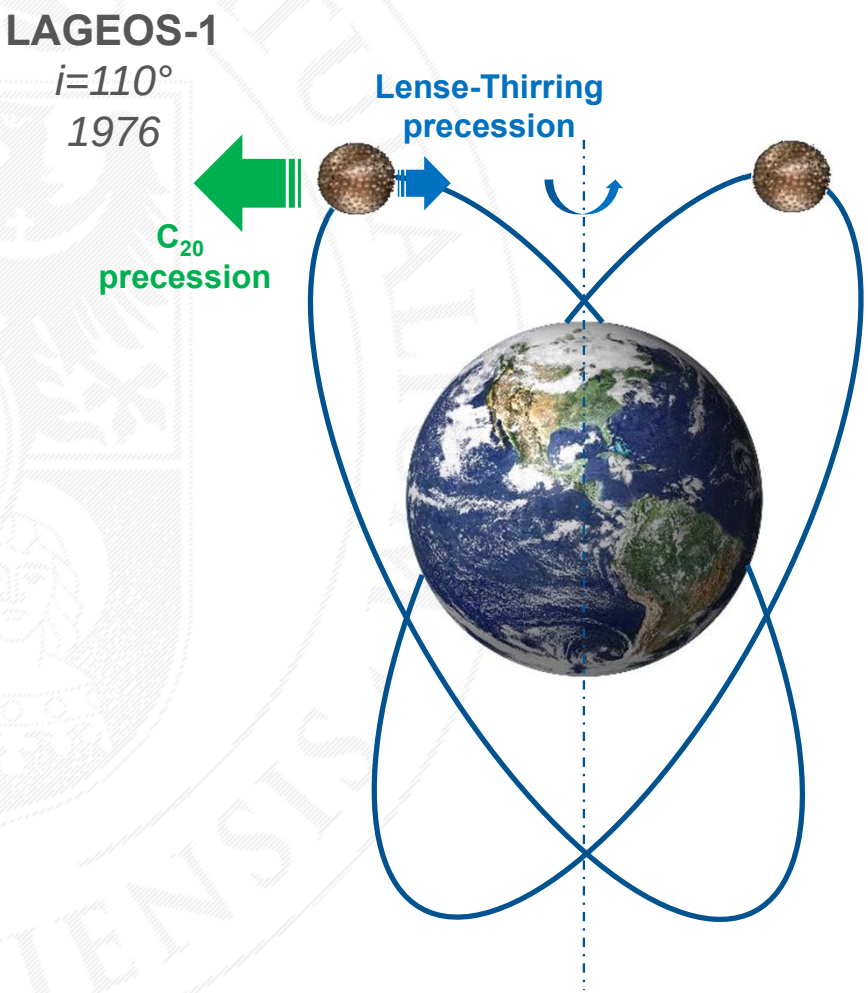

LAGEOS-2
i=70°

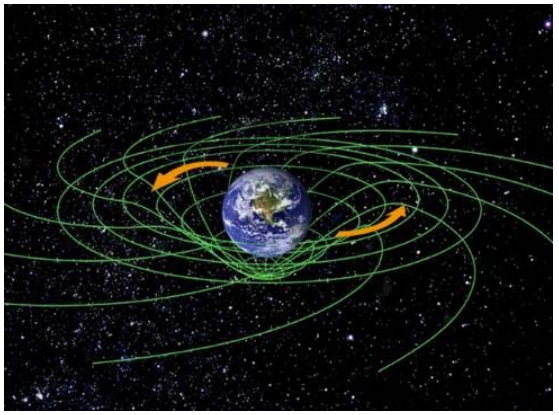

Lense-Thirring

$$\Delta\Omega_{LT} = 2\frac{GM_{\oplus}J_{\oplus}}{c^2a^3(1-e^2)^{\frac{3}{2}}}\Delta t$$

$$\Delta\Omega_{C_{20}} = -\frac{3}{2}\sqrt{\frac{GM_{\oplus}}{r_{\oplus}^3}}\left(\frac{r_{\oplus}}{a}\right)^{\frac{7}{2}}\frac{\cos(i)}{(1-e^2)^2}C_{2,0}\,\Delta t$$

Lense-Thirring effect – confirmation using geodetic satellites

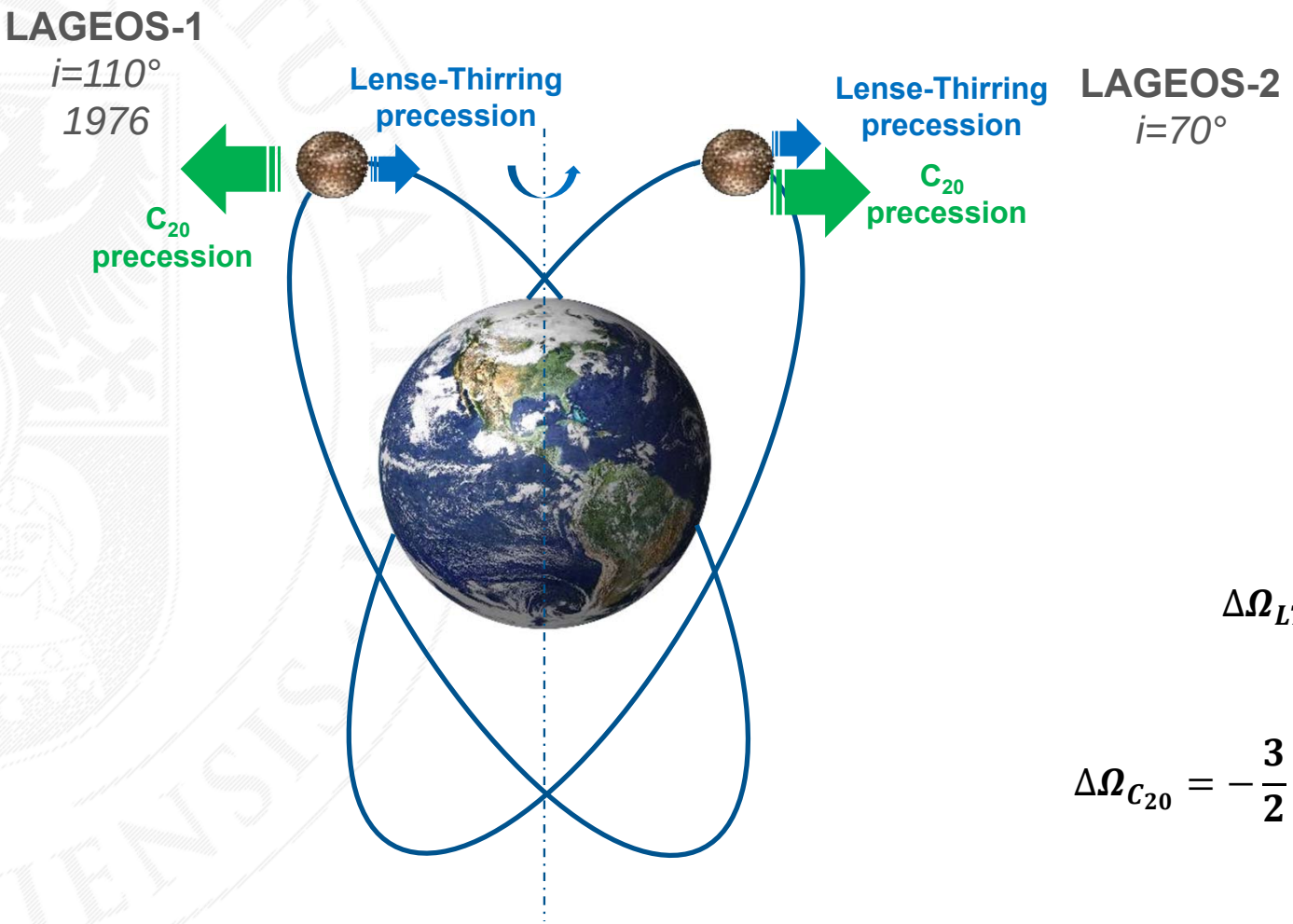

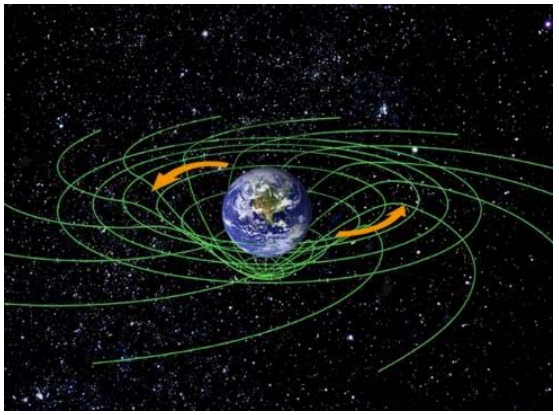

Lense-Thirring

$$\Delta\Omega_{LT} = 2\frac{GM_{\oplus}J_{\oplus}}{c^2a^3(1-e^2)^{\frac{3}{2}}}\Delta t$$

$$\Delta\Omega_{C_{20}} = -\frac{3}{2}\sqrt{\frac{GM_{\oplus}}{r_{\oplus}^3}}\left(\frac{r_{\oplus}}{a}\right)^{\frac{7}{2}}\frac{\cos(i)}{(1-e^2)^2}C_{2,0}\,\Delta t$$

Lense-Thirring effect – confirmation using geodetic satellites

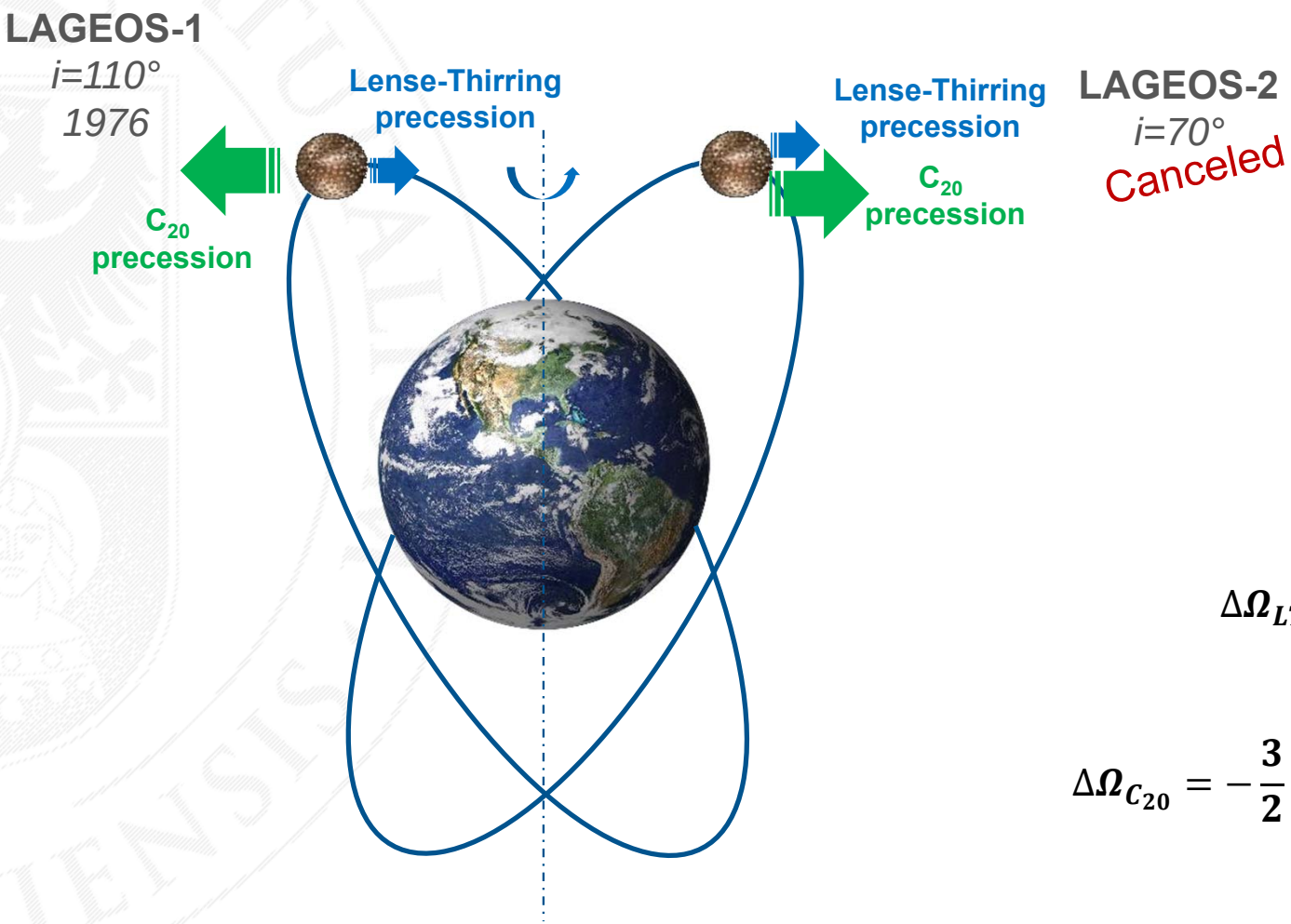

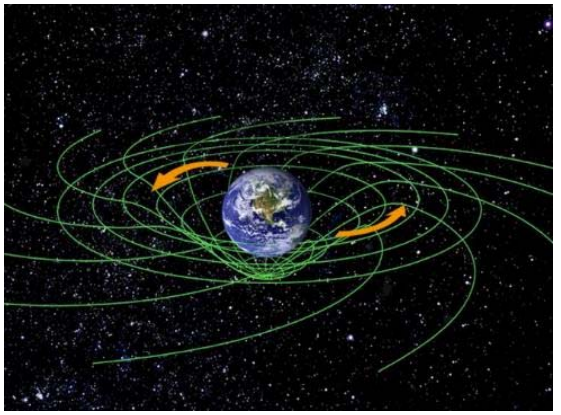

Lense-Thirring

$$\Delta\Omega_{LT} = 2\frac{GM_{\oplus}J_{\oplus}}{c^2a^3(1-e^2)^{\frac{3}{2}}}\Delta t$$

$$\Delta\Omega_{C_{20}} = -\frac{3}{2}\sqrt{\frac{GM_{\oplus}}{r_{\oplus}^3}}\left(\frac{r_{\oplus}}{a}\right)^{\frac{7}{2}}\frac{\cos(i)}{(1-e^2)^2}C_{2,0}\,\Delta t$$

Lense-Thirring effect – confirmation using geodetic satellites

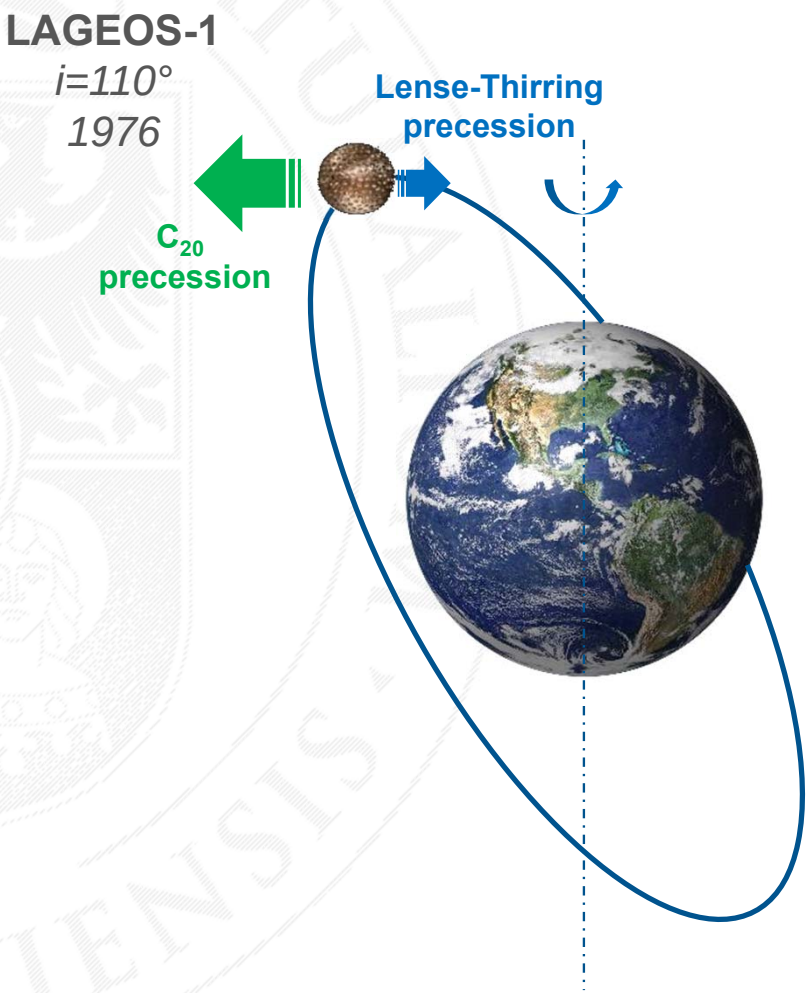

LAGEOS-2
i=70°
Canceled

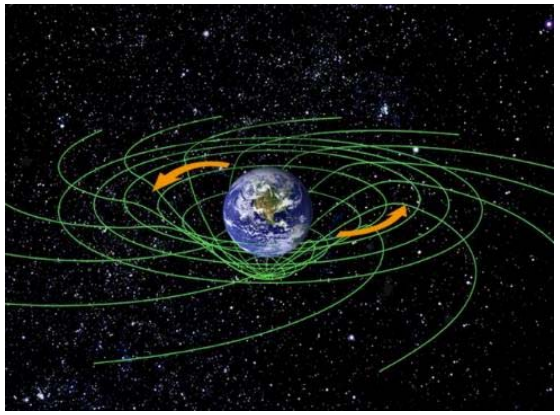

Lense-Thirring

$$\Delta\Omega_{LT} = 2\frac{GM_{\oplus}J_{\oplus}}{c^2a^3(1-e^2)^{\frac{3}{2}}}\Delta t$$

$$\Delta\Omega_{C_{20}} = -\frac{3}{2}\sqrt{\frac{GM_{\oplus}}{r_{\oplus}^3}}\left(\frac{r_{\oplus}}{a}\right)^{\frac{7}{2}}\frac{\cos(i)}{(1-e^2)^2}C_{2,0}\,\Delta t$$

Lense-Thirring effect – confirmation using geodetic satellites

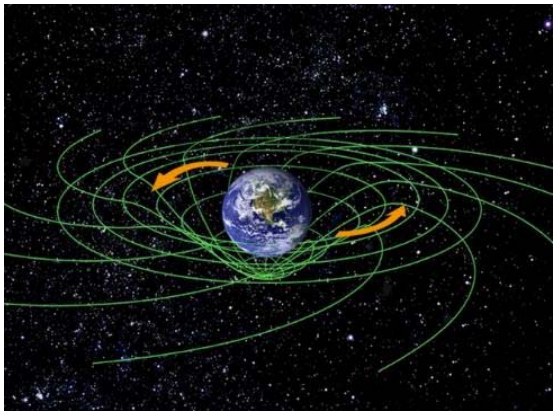

Lense-Thirring

LAGEOS-1
i=110°
1976

Lense-Thirring precession

C_{20} precession

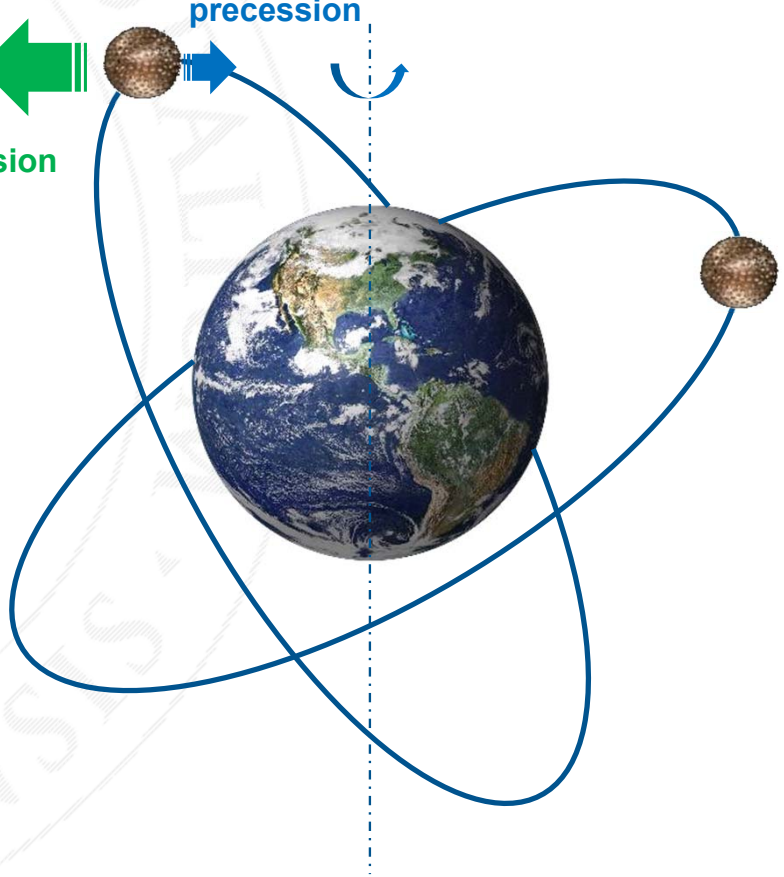

LAGEOS-2
i=70°
Canceled

LAGEOS-2
i=52.6°
1992

$$\Delta\Omega_{LT} = 2\frac{GM_{\oplus}J_{\oplus}}{c^2a^3(1-e^2)^{\frac{3}{2}}}\Delta t$$

$$\Delta\Omega_{C_{20}} = -\frac{3}{2}\sqrt{\frac{GM_{\oplus}}{r_{\oplus}^3}}\left(\frac{r_{\oplus}}{a}\right)^{\frac{7}{2}}\frac{\cos(i)}{(1-e^2)^2}C_{2,0}\,\Delta t$$

Lense-Thirring effect – confirmation using geodetic satellites

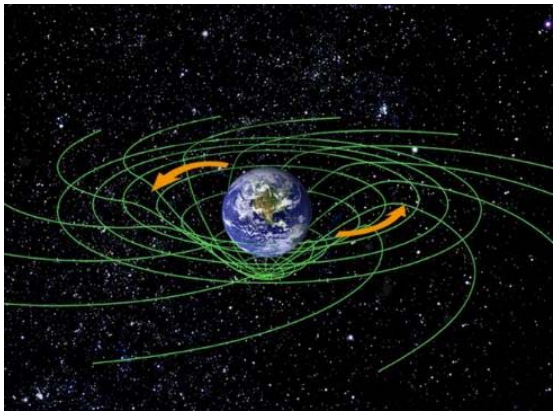

Lense-Thirring

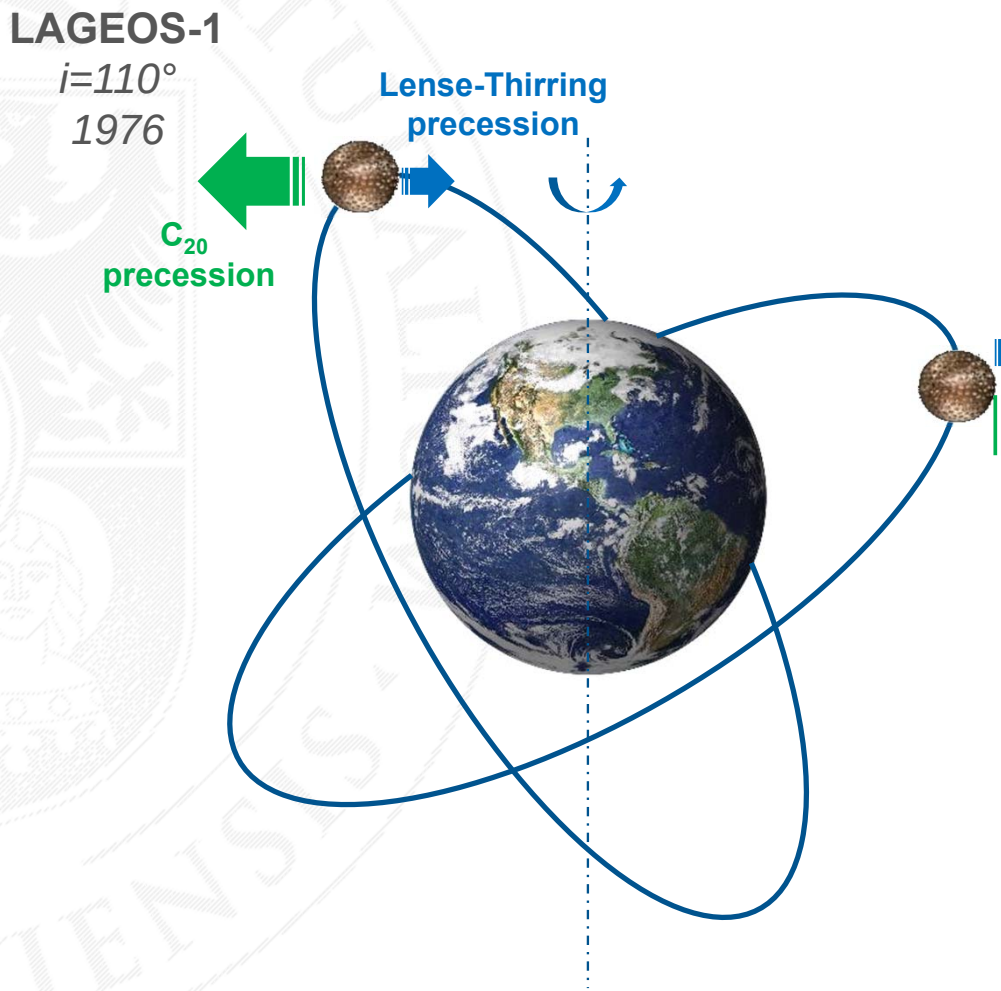

$$\Delta\Omega_{LT} = 2\frac{GM_{\oplus}J_{\oplus}}{c^2a^3(1-e^2)^{\frac{3}{2}}}\Delta t$$

$$\Delta\Omega_{C_{20}} = -\frac{3}{2}\sqrt{\frac{GM_{\oplus}}{r_{\oplus}^3}}\left(\frac{r_{\oplus}}{a}\right)^{\frac{7}{2}}\frac{\cos(i)}{(1-e^2)^2}C_{2,0}\,\Delta t$$

Lense-Thirring effect – confirmation using geodetic satellites

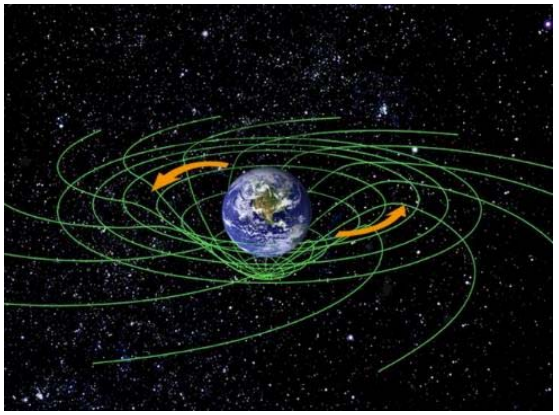

Lense-Thirring

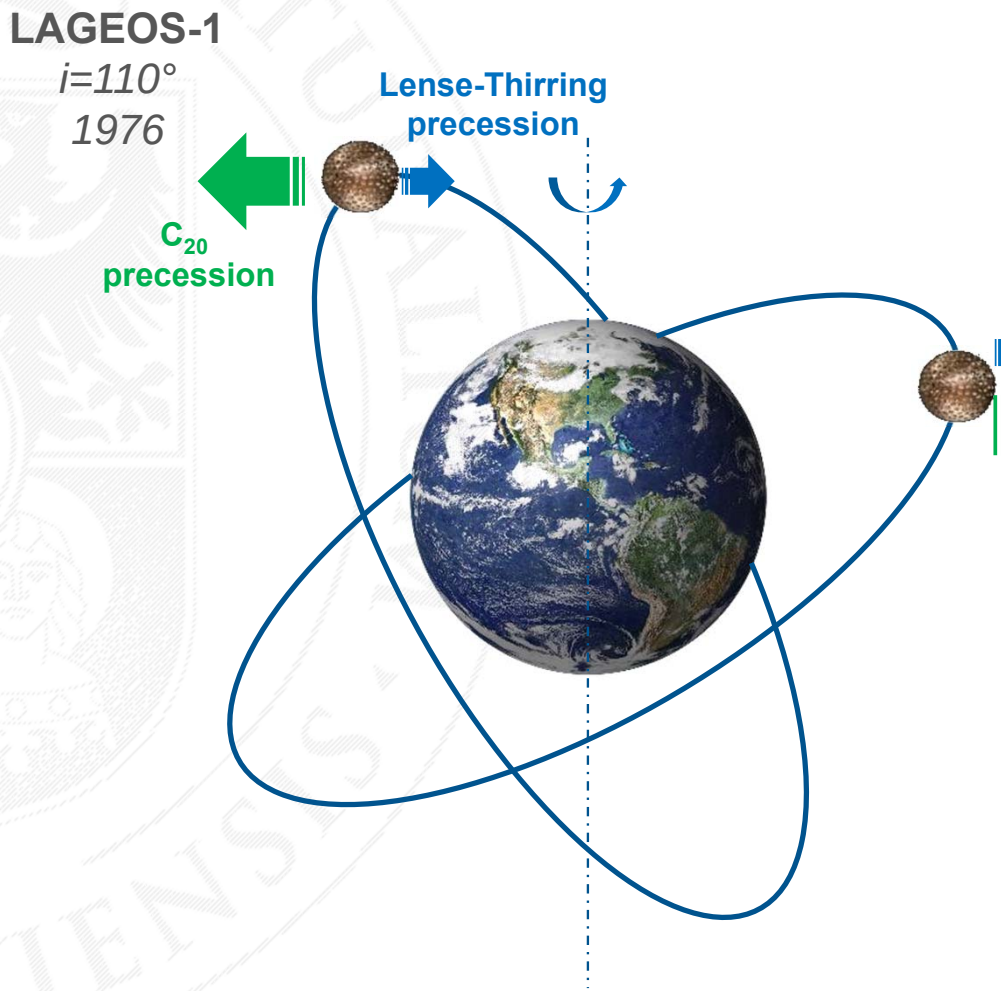

$$\Delta\Omega_{LT} = 2\frac{GM_{\oplus}J_{\oplus}}{c^2a^3(1-e^2)^{\frac{3}{2}}}\Delta t$$

$$\Delta\Omega_{C_{20}} = -\frac{3}{2}\sqrt{\frac{GM_{\oplus}}{r_{\oplus}^3}}\left(\frac{r_{\oplus}}{a}\right)^{\frac{7}{2}}\frac{\cos(i)}{(1-e^2)^2}C_{2,0}\,\Delta t$$

Lense-Thirring effect – confirmation using geodetic satellites

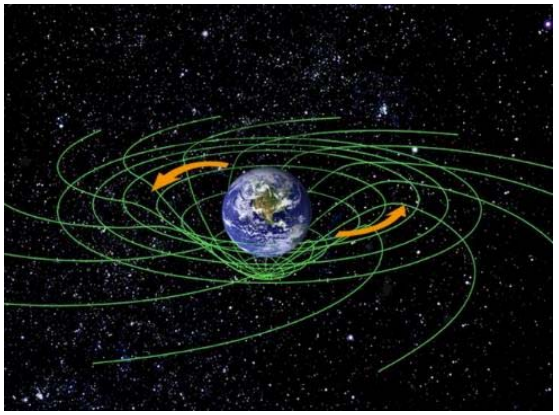

Lense-Thirring

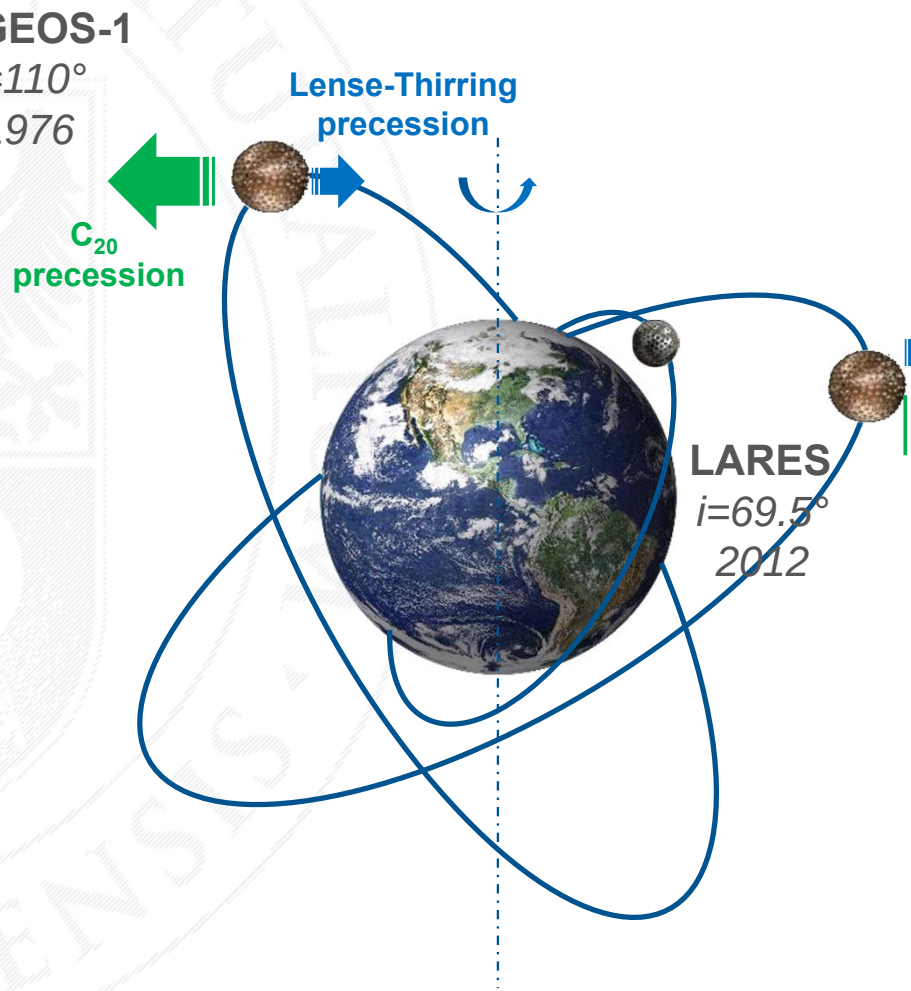

$$\Delta\Omega_{LT} = 2\frac{GM_{\oplus}J_{\oplus}}{c^2a^3(1-e^2)^{\frac{3}{2}}}\Delta t$$

$$\Delta\Omega_{C_{20}} = -\frac{3}{2}\sqrt{\frac{GM_{\oplus}}{r_{\oplus}^3}}\left(\frac{r_{\oplus}}{a}\right)^{\frac{7}{2}}\frac{\cos(i)}{(1-e^2)^2}C_{2,0}\,\Delta t$$

Lense-Thirring effect – confirmation using geodetic satellites

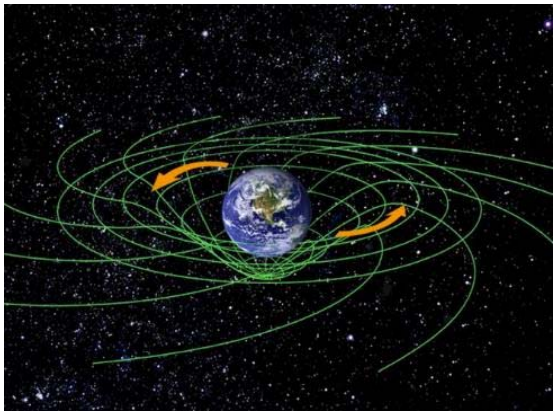

Lense-Thirring

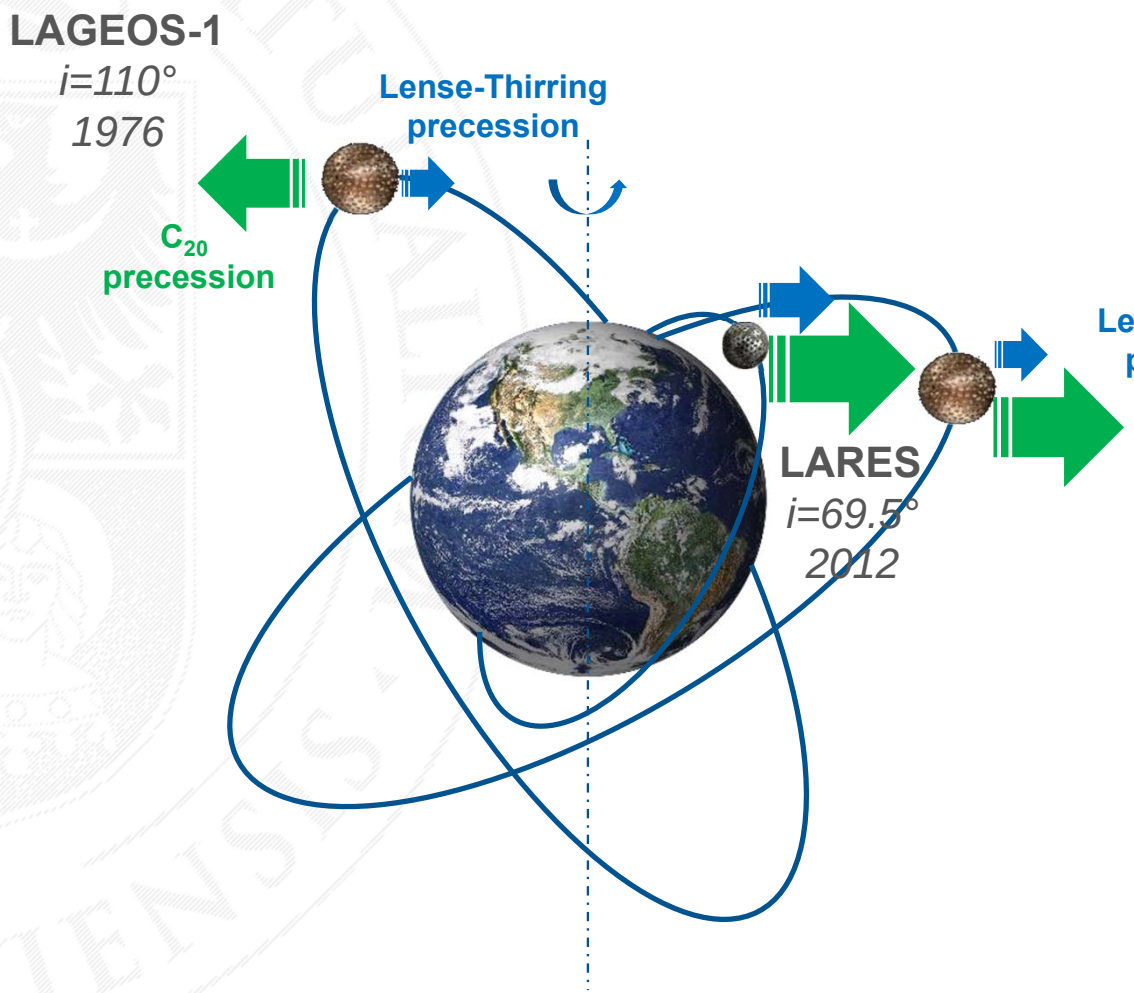

$$\Delta\Omega_{LT} = 2\frac{GM_{\oplus}J_{\oplus}}{c^2a^3(1-e^2)^{\frac{3}{2}}}\Delta t$$

$$\Delta\Omega_{C_{20}} = -\frac{3}{2}\sqrt{\frac{GM_{\oplus}}{r_{\oplus}^3}}\left(\frac{r_{\oplus}}{a}\right)^{\frac{7}{2}}\frac{\cos(i)}{(1-e^2)^2}C_{2,0}\,\Delta t$$

Lense-Thirring effect – confirmation using geodetic satellites

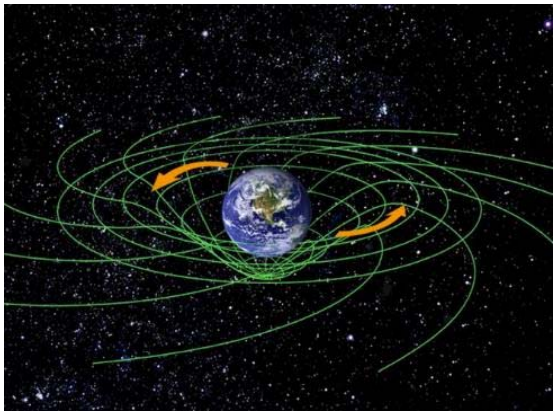

Lense-Thirring

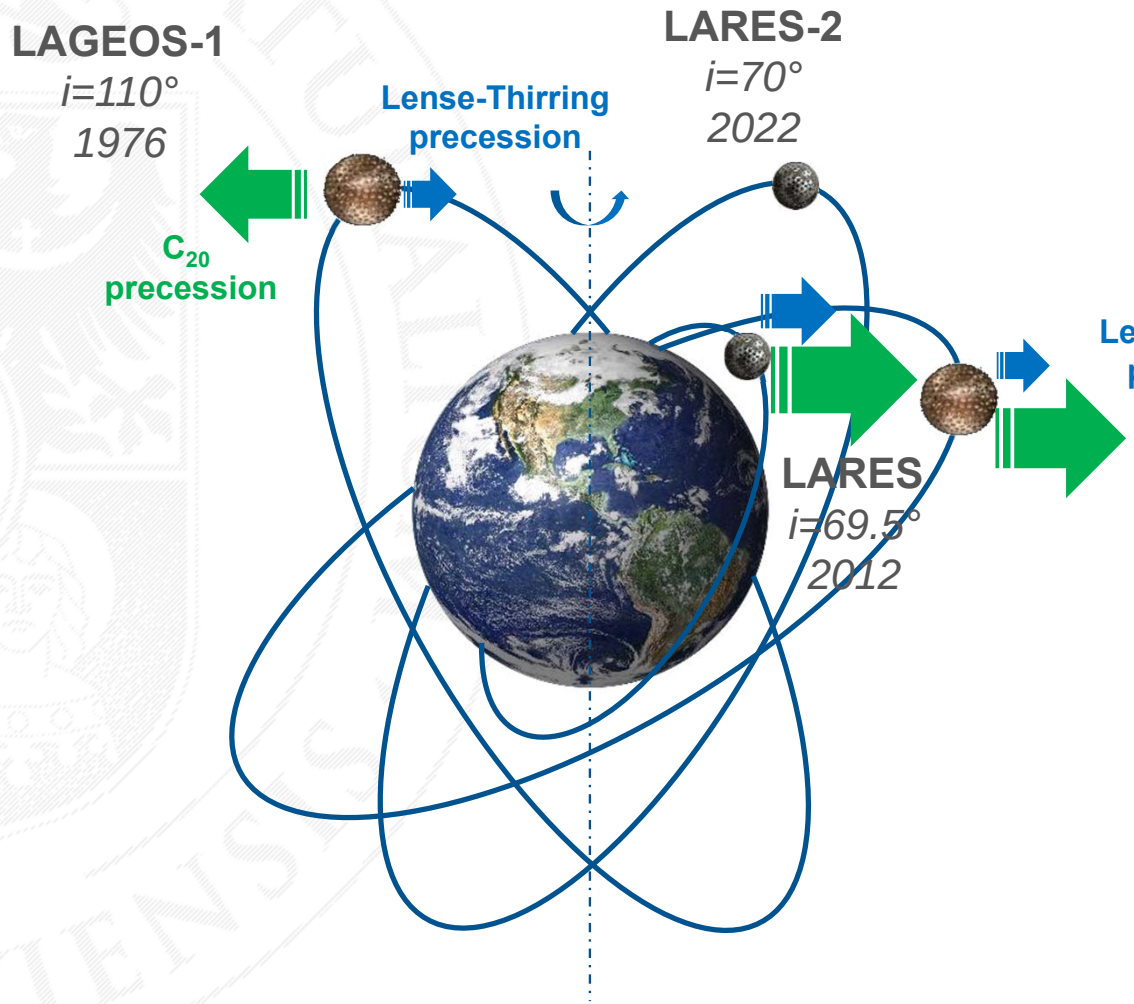

$$\Delta\Omega_{LT} = 2\frac{GM_{\oplus}J_{\oplus}}{c^2a^3(1-e^2)^{\frac{3}{2}}}\Delta t$$

$$\Delta\Omega_{C_{20}} = -\frac{3}{2}\sqrt{\frac{GM_{\oplus}}{r_{\oplus}^3}}\left(\frac{r_{\oplus}}{a}\right)^{\frac{7}{2}}\frac{\cos(i)}{(1-e^2)^2}C_{2,0}\,\Delta t$$

Lense-Thirring effect – confirmation using geodetic satellites

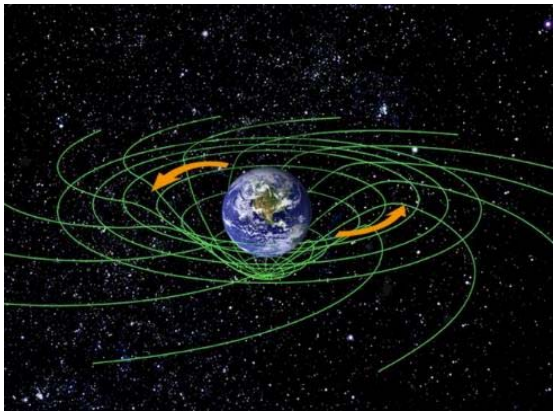

Lense-Thirring

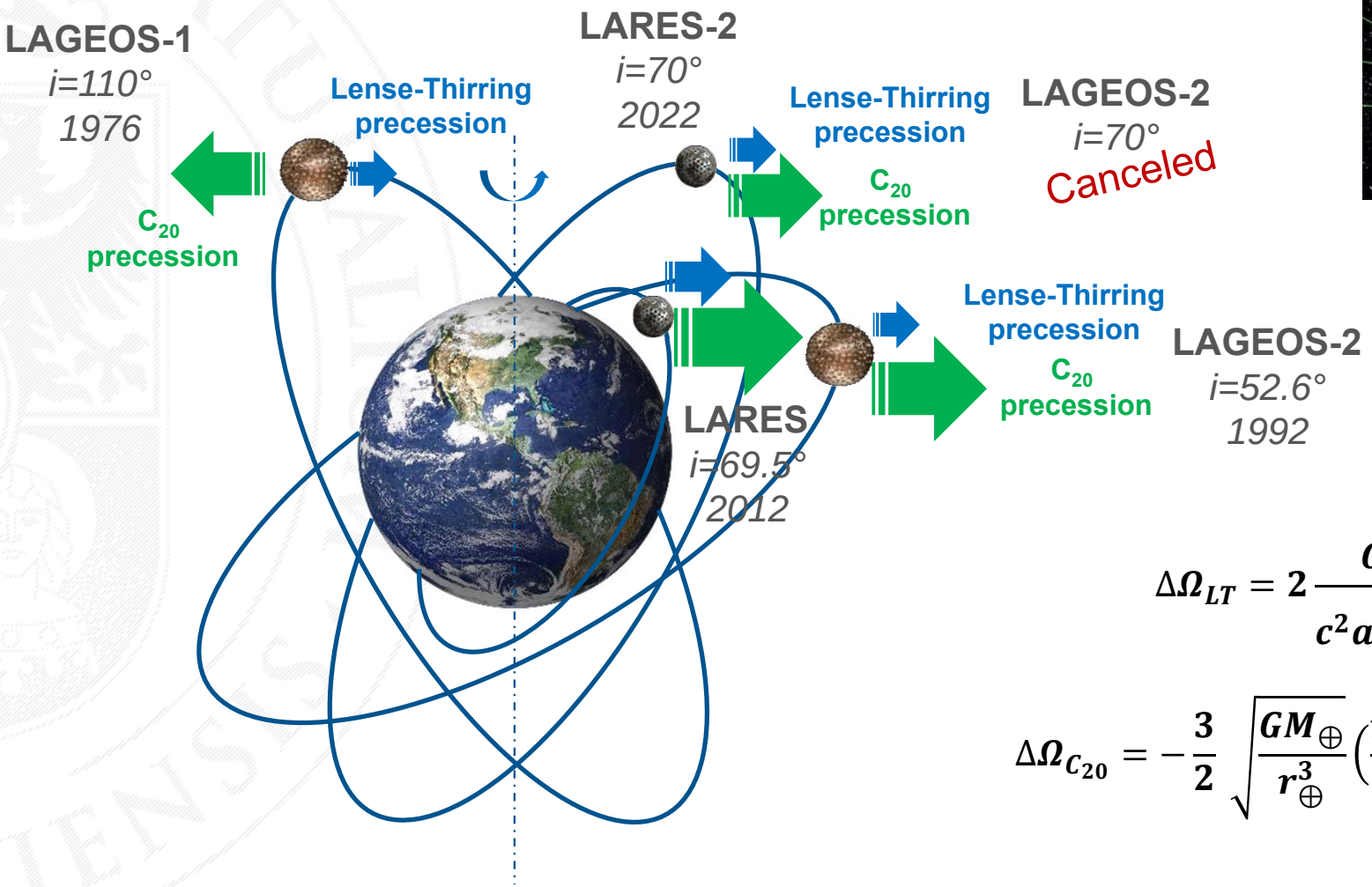

$$\Delta\Omega_{LT} = 2\frac{GM_{\oplus}J_{\oplus}}{c^2a^3(1-e^2)^{\frac{3}{2}}}\Delta t$$

$$\Delta\Omega_{C_{20}} = -\frac{3}{2}\sqrt{\frac{GM_{\oplus}}{r_{\oplus}^3}}\left(\frac{r_{\oplus}}{a}\right)^{\frac{7}{2}}\frac{\cos(i)}{(1-e^2)^2}C_{2,0}\,\Delta t$$

LARES-2 – basic parameters

	LAGEOS-1	LAGEOS-2	LARES-1	LARES-2
Launch date	1976	1992	2013	2022
Sponsor	NASA	NASA/ASI	ASI/ESA	ASI/ESA
ILRS number	L51	L52	L60	L67
Material (alloy)	brass/ aluminum	brass/ aluminum	tungsten	nickel
Altitude (km)	**5860**	**5620**	**1440**	**5880**
Inclination (°)	109.9	52.6	69.6	70.1
Eccentricity	0.0039	0.0137	0.0008	0.0002
Mass (kg)	**407**	**405**	**386.8**	**297.5**
Area-to-mass ratio (e-4 m^2/kg)	**6.9**	**7.0**	2.7	**4.7**
Center-of-mass (approx.) (mm)	251	251	133	137.1
Radius (mm)	**300**	**300**	**182**	**212**
Corner cubes	426	426	**92**	**303**
SRP coefficient C_R	1.13	1.13	1.08	1.08
Draconitic year	560	222	133	270

Processing period:
July 2022 – January 2024

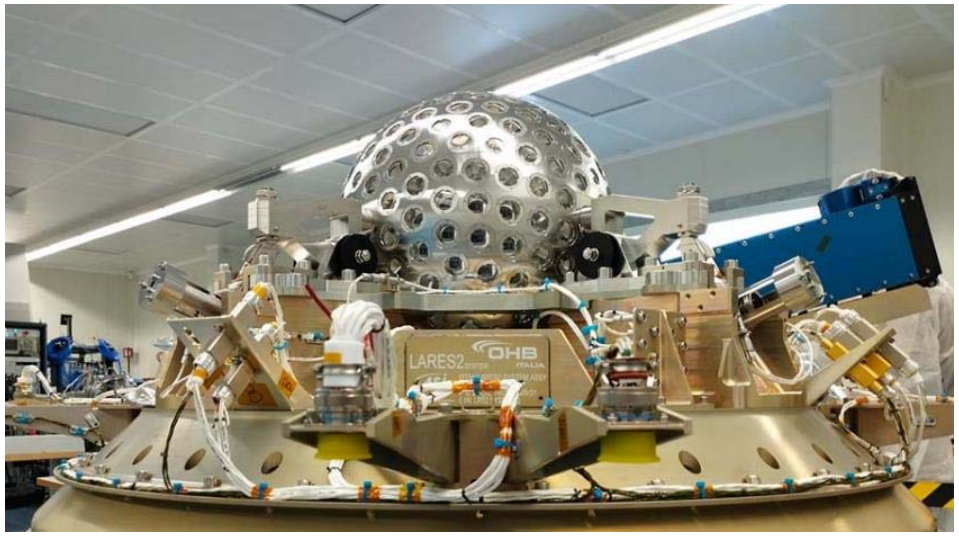

LARES-2, courtesy of ASI

- **The area-to-mass ratio for LARES-2 is smaller by 32% compared to LAGEOS-1/2 – implying smaller non-gravitational orbit perturbations.**
- **Solid sphere with no inner structure (as opposed to LAGEOS-1/2)**
- **Center-of-mass corrections well defined with small spread between different detectors**

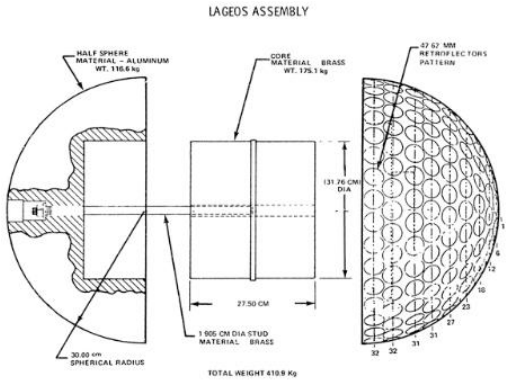

LAGEOS assembly, courtesy of NASA

Observation residuals

mean +/- STD

LARES-2

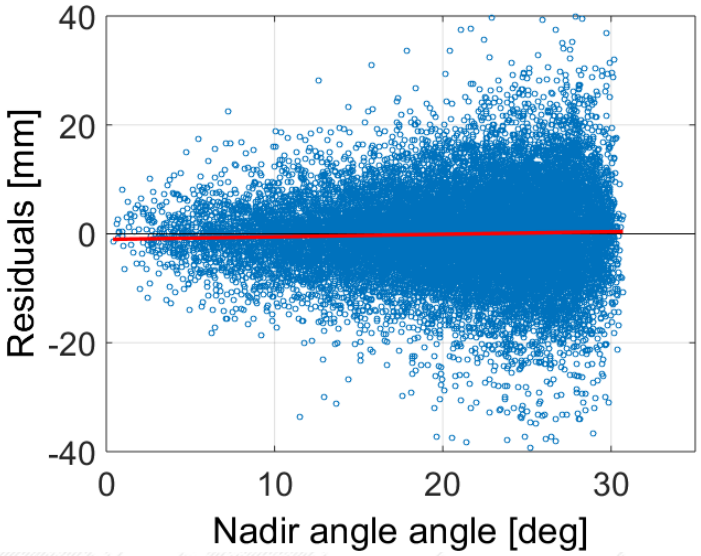

-0.03 +/- 8.04 mm

LAGEOS-1

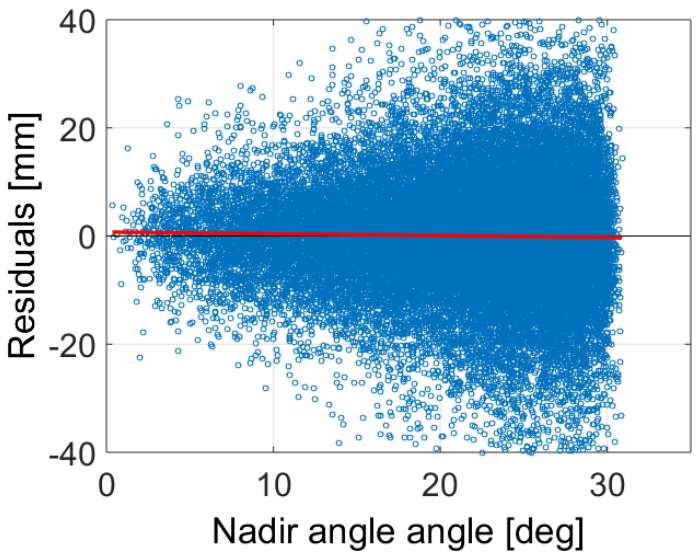

0.02 +/- 10.89 mm

LAGEOS-2

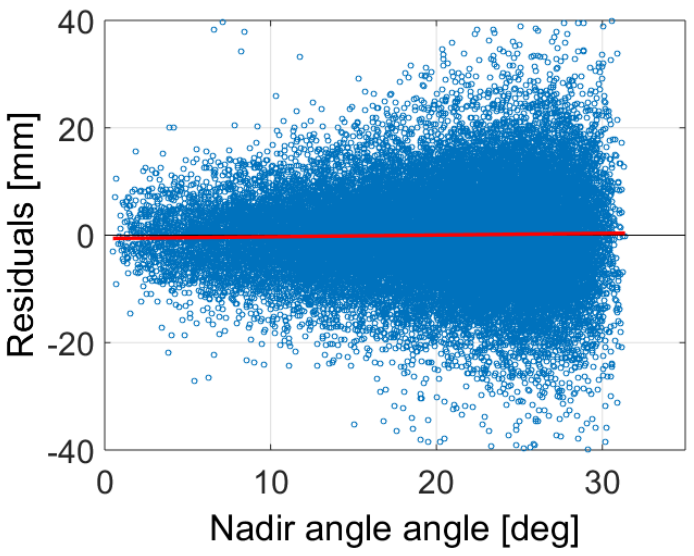

0.03 +/- 8.73 mm

The spread of SLR residuals for LARES-2 is about 26% smaller than that for LAGEOS-1 (smaller area-to-mass ratio, better orbits, smaller spread of center-of-mass corrections).

Geocenter coordinates - formal errors

Once-per-revolution (OPR) empirical orbit parameters in along-track **S_C/S_S reduce the formal errors for the X and Y** components, but **increase for the Z component** (due to correlations).

LARES-2 does not require estimation of OPR when gravity field is estimated (due to small sensitivity to thermal effects).

LARES-2 reduces the formal errors of the Z geocenter component by up to 59%.

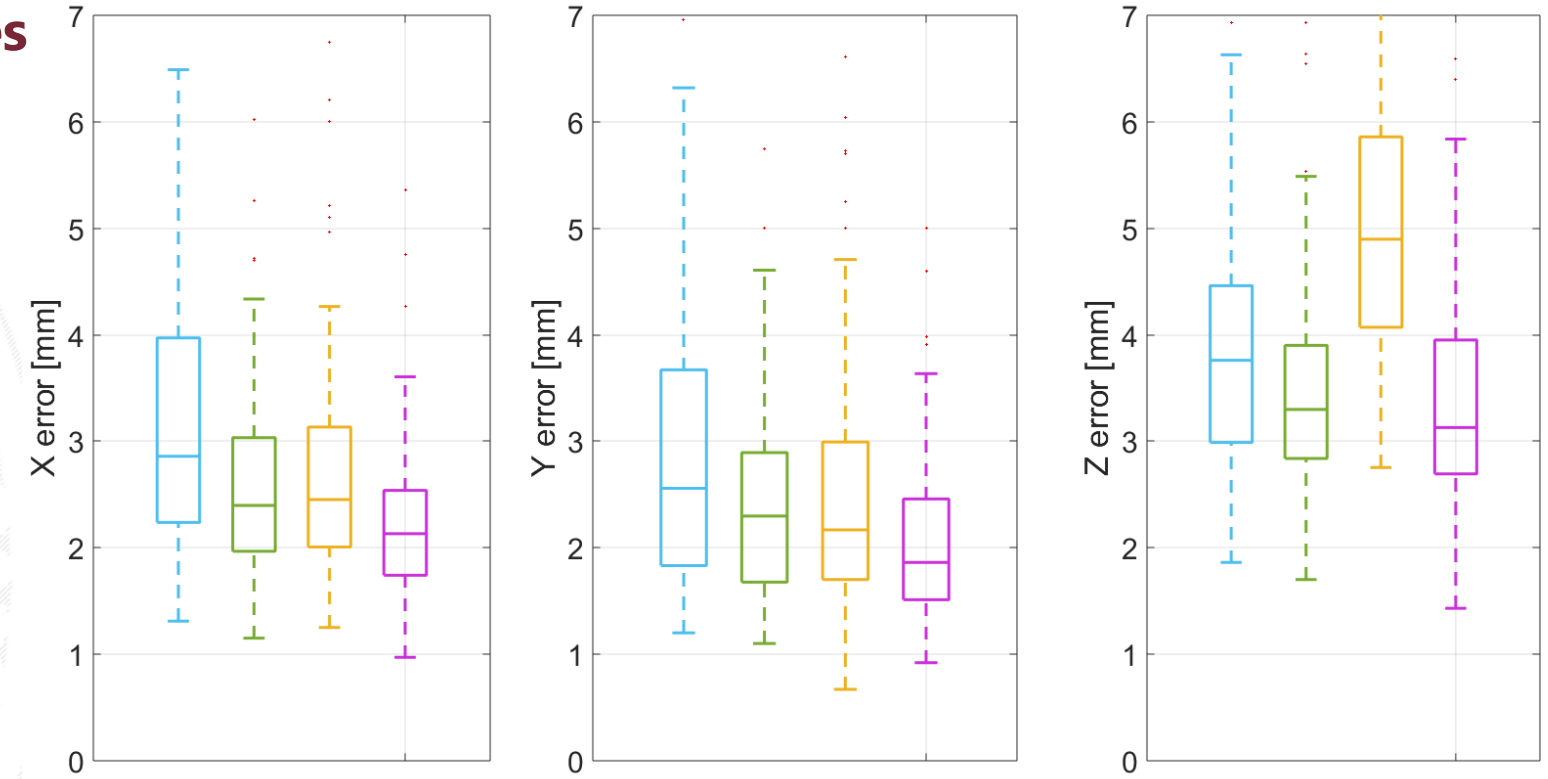

Solution	LAGEOS-1	LAGEOS-2	LARES-2	Gravity field
LAG grav 3x3 no OPR	S_0, D_0	S_0, D_0	n/a	d/o 3x3
LAG+LAR grav 3x3 no OPR	**S_0, D_0**	**S_0, D_0**	**S_0, D_0**	d/o 3x3
LAG grav 3x3 + OPR	S_0, S_C, S_S	S_0, S_C, S_S	n/a	d/o 3x3
LAG+LAR grav 3x3 + OPR for LAG	**S_0, S_C, S_S**	**S_0, S_C, S_S**	**S_0**	d/o 3x3

Geocenter coordinates - formal errors

Once-per-revolution (OPR) empirical orbit parameters in along-track **S_C/S_S reduce the formal errors for the X and Y** components, but **increase for the Z component** (due to correlations).

LARES-2 does not require estimation of OPR when gravity field is estimated (due to small sensitivity to thermal effects).

LARES-2 reduces the formal errors of the Z geocenter component by up to 59%.

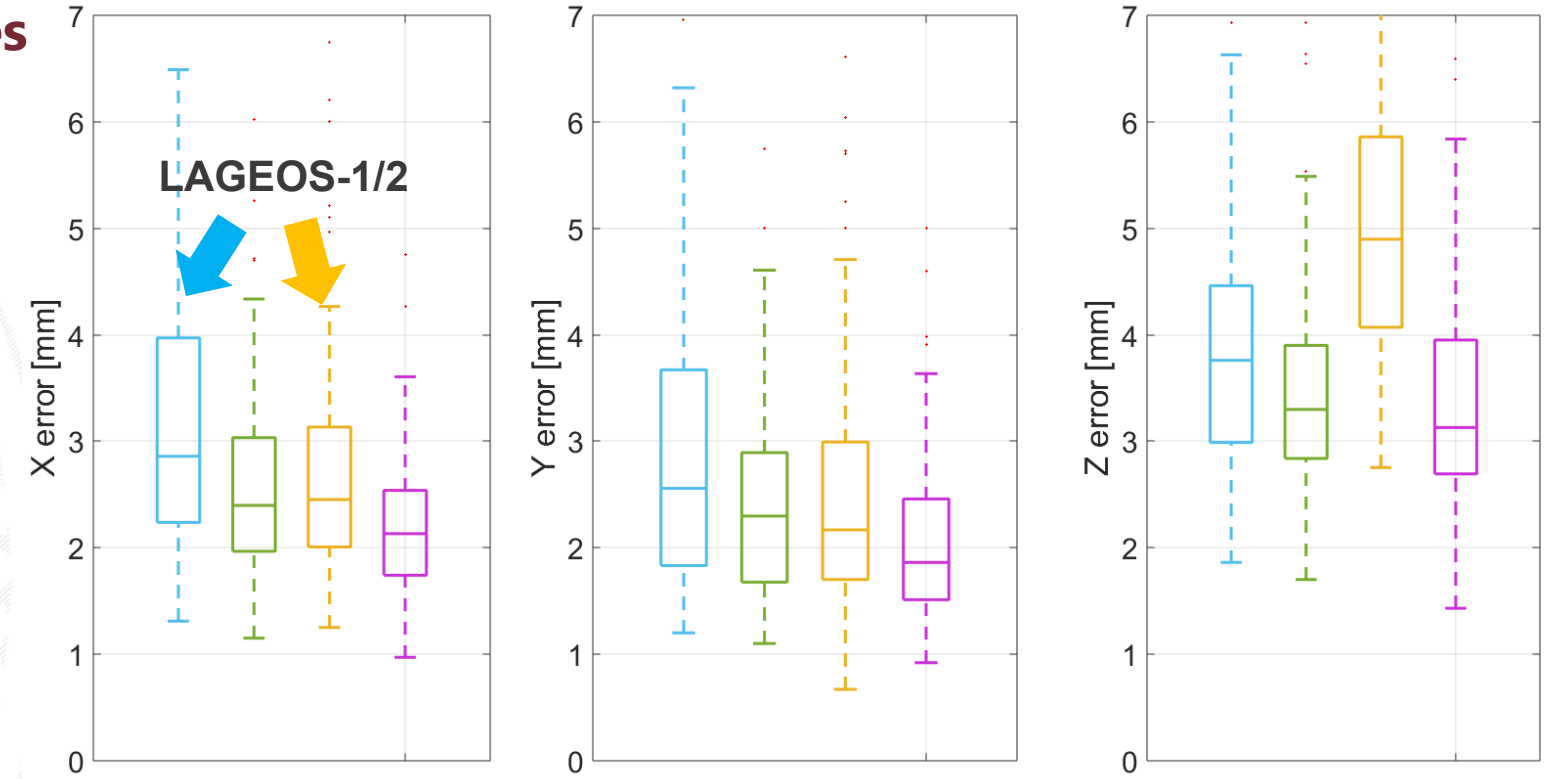

Solution	LAGEOS-1	LAGEOS-2	LARES-2	Gravity field
LAG grav 3x3 no OPR	S_0, D_0	S_0, D_0	n/a	d/o 3x3
LAG+LAR grav 3x3 no OPR	**S_0, D_0**	**S_0, D_0**	**S_0, D_0**	d/o 3x3
LAG grav 3x3 + OPR	S_0, S_C, S_S	S_0, S_C, S_S	n/a	d/o 3x3
LAG+LAR grav 3x3 + OPR for LAG	**S_0, S_C, S_S**	**S_0, S_C, S_S**	**S_0**	d/o 3x3

Geocenter coordinates - formal errors

Once-per-revolution (OPR) empirical orbit parameters in along-track **S_C/S_S reduce the formal errors for the X and Y** components, but **increase for the Z component** (due to correlations).

LARES-2 does not require estimation of OPR when gravity field is estimated (due to small sensitivity to thermal effects).

LARES-2 reduces the formal errors of the Z geocenter component by up to 59%.

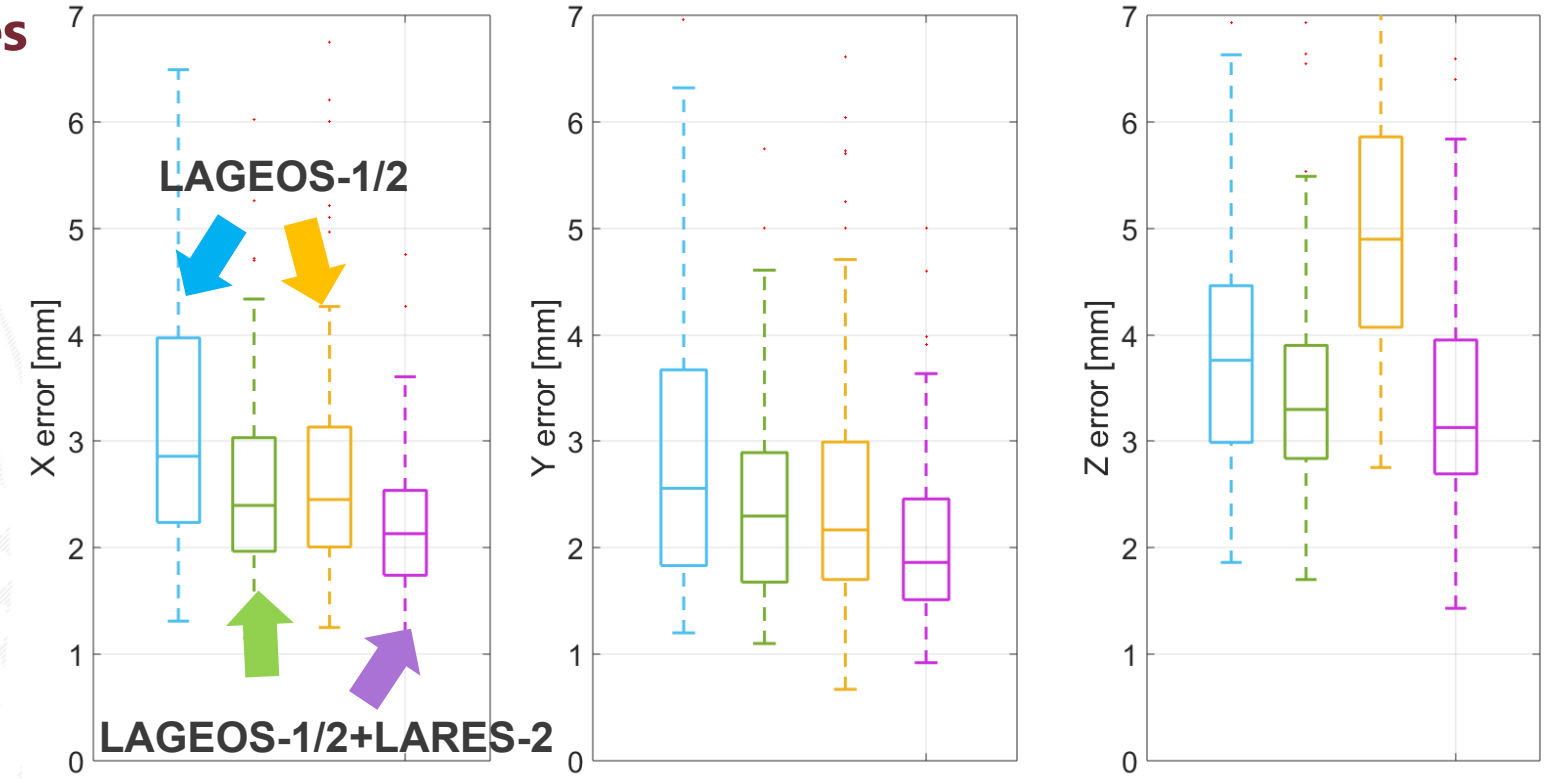

Solution	LAGEOS-1	LAGEOS-2	LARES-2	Gravity field
LAG grav 3x3 no OPR	S_0, D_0	S_0, D_0	n/a	d/o 3x3
LAG+LAR grav 3x3 no OPR	**S_0, D_0**	**S_0, D_0**	**S_0, D_0**	d/o 3x3
LAG grav 3x3 + OPR	S_0, S_C, S_S	S_0, S_C, S_S	n/a	d/o 3x3
LAG+LAR grav 3x3 + OPR for LAG	**S_0, S_C, S_S**	**S_0, S_C, S_S**	**S_0**	d/o 3x3

Geocenter coordinates - formal errors

Once-per-revolution (OPR) empirical orbit parameters in along-track S_C/S_S **reduce the formal errors for the X and Y** components, but **increase for the Z component** (due to correlations).

LARES-2 does not require estimation of OPR when gravity field is estimated (due to small sensitivity to thermal effects).

LARES-2 reduces the formal errors of the Z geocenter component by up to 59%.

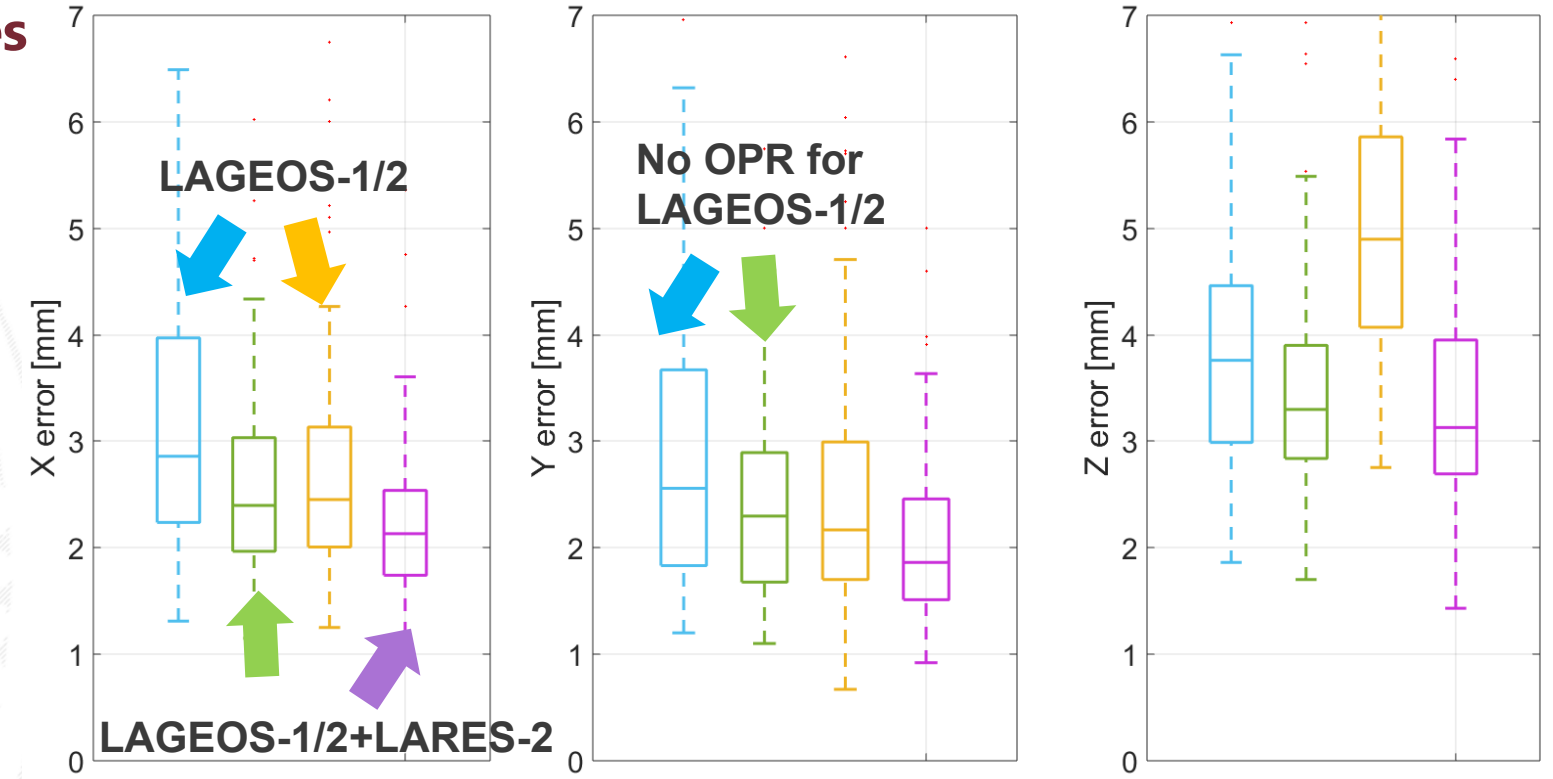

Solution	LAGEOS-1	LAGEOS-2	LARES-2	Gravity field
LAG grav 3x3 no OPR	S_0, D_0	S_0, D_0	n/a	d/o 3x3
LAG+LAR grav 3x3 no OPR	**S_0, D_0**	**S_0, D_0**	**S_0, D_0**	d/o 3x3
LAG grav 3x3 + OPR	S_0, S_C, S_S	S_0, S_C, S_S	n/a	d/o 3x3
LAG+LAR grav 3x3 + OPR for LAG	**S_0, S_C, S_S**	**S_0, S_C, S_S**	**S_0**	d/o 3x3

Geocenter coordinates - formal errors

Once-per-revolution (OPR) empirical orbit parameters in along-track S_C/S_S **reduce the formal errors for the X and Y** components, but **increase for the Z component** (due to correlations).

LARES-2 does not require estimation of OPR when gravity field is estimated (due to small sensitivity to thermal effects).

LARES-2 reduces the formal errors of the Z geocenter component by up to 59%.

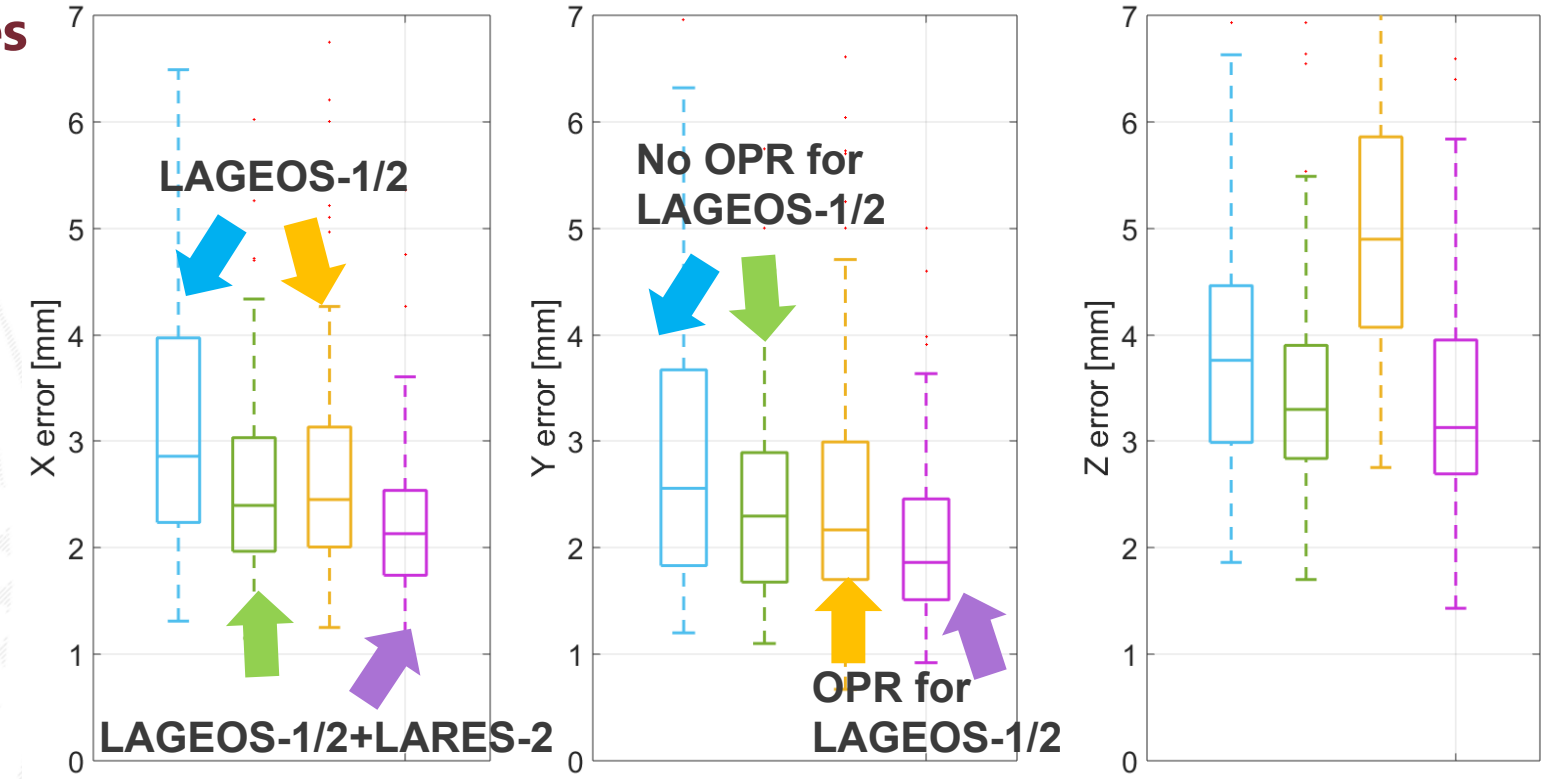

Solution	LAGEOS-1	LAGEOS-2	LARES-2	Gravity field
LAG grav 3x3 no OPR	S_0, D_0	S_0, D_0	n/a	d/o 3x3
LAG+LAR grav 3x3 no OPR	**S_0, D_0**	**S_0, D_0**	**S_0, D_0**	d/o 3x3
LAG grav 3x3 + OPR	S_0, S_C, S_S	S_0, S_C, S_S	n/a	d/o 3x3
LAG+LAR grav 3x3 + OPR for LAG	**S_0, S_C, S_S**	**S_0, S_C, S_S**	**S_0**	d/o 3x3

Geocenter coordinates - estimates

The most stable solution is no. 4 with LARES-2 and OPR estimated for LAGEOS-1/2.

The least stable Z geocenter is derived from no. 3 with the estimation OPR for LAGEOS-1/2.

Minor LARES-2 impact is observed for solutions without OPR for LAGEOS (no. 1 and 2).

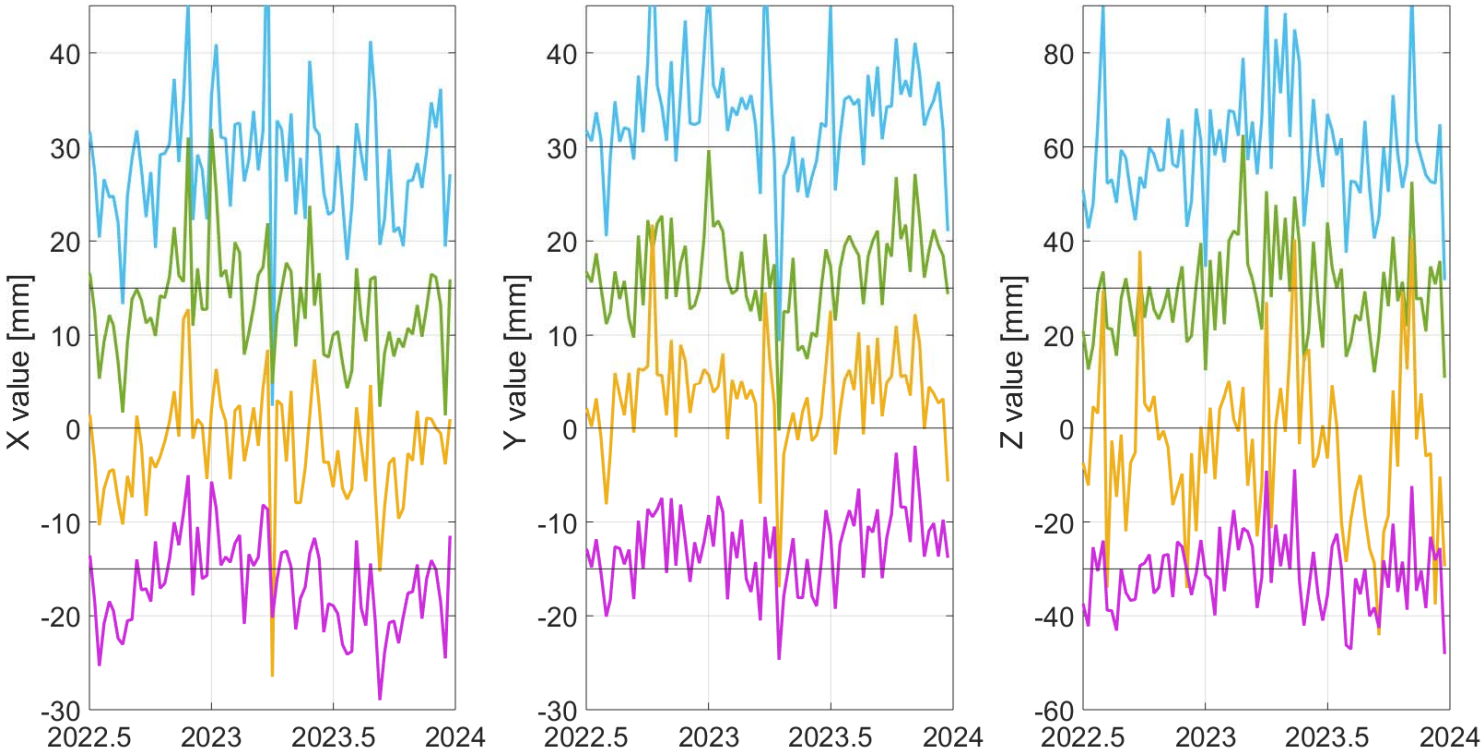

Solution	LAGEOS-1	LAGEOS-2	LARES-2	Gravity field
LAG grav 3x3 no OPR	S_0, D_0	S_0, D_0	n/a	d/o 3x3
LAG+LAR grav 3x3 no OPR	**S_0, D_0**	**S_0, D_0**	**S_0, D_0**	d/o 3x3
LAG grav 3x3 + OPR	S_0, S_C, S_S	S_0, S_C, S_S	n/a	d/o 3x3
LAG+LAR grav 3x3 + OPR for LAG	**S_0, S_C, S_S**	**S_0, S_C, S_S**	**S_0**	d/o 3x3

Gravity field – C_{20}

C_{20} Median errors are:
6.75 6.26 9.82 5.93 ($\cdot 10^{-12}$).

LARES-2 reduces the C_{20} formal errors by up to 40% and reduces the spread for the solution with OPR estimated for LAGEOS.

C_{20} estimates are quite consistent in all solutions.

LAG grav 3x3 no OPR

LAG+LAR grav 3x3 no OPR

LAG grav 3x3 + OPR

LAG+LAR grav 3x3 + OPR for LAG

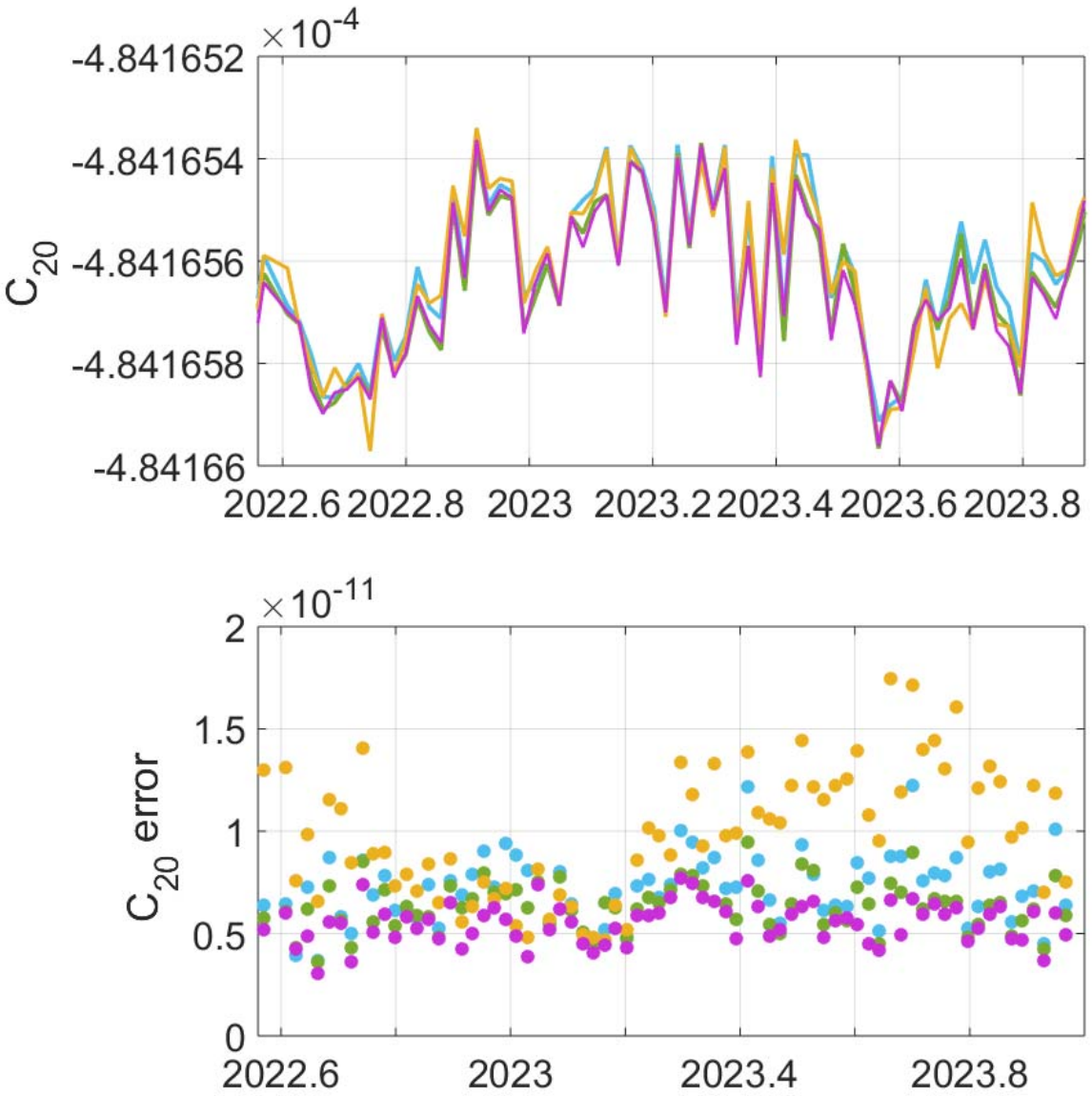

Gravity field – C_{30}

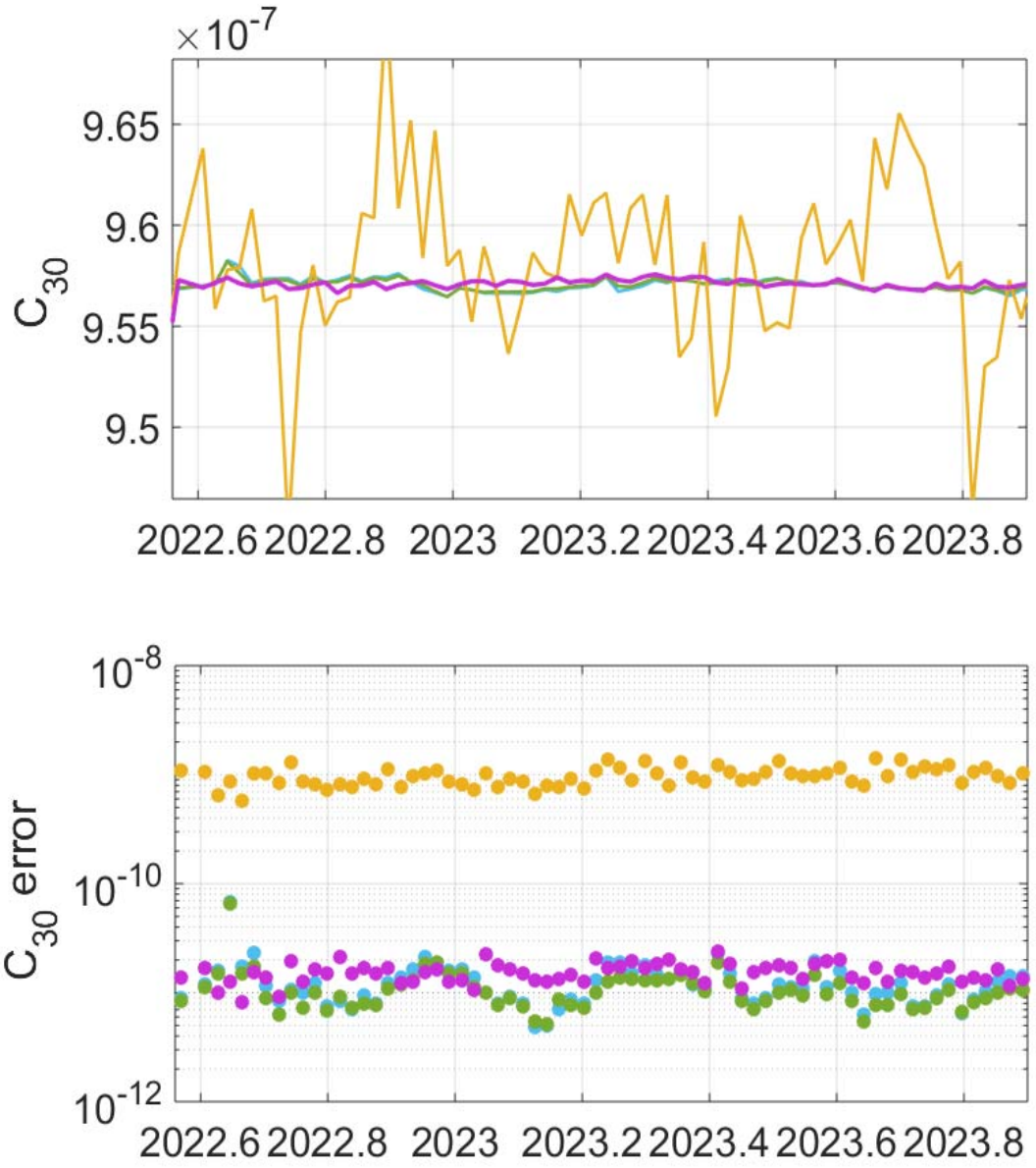

LAG grav 3x3 no OPR

LAG+LAR grav 3x3 no OPR

LAG grav 3x3 + OPR

LAG+LAR grav 3x3 + OPR for LAG

Gravity field – C_{30}

Unrealistic C_{30} signal in no. 3 when estimating OPR for LAGEOS-1/2 (due to correlations) and not including LARES-2.

When not estimating OPR for LAGEOS in no. 1 and 2, the C_{30} estimated are affected by unmodeled thermal effects (Yarkovsky and Yarkovsky Schach).

The only reasonable solution is no. 4 with LARES-2 included and OPR for LAGEOS-1/2.

- LAG grav 3x3 no OPR
- LAG+LAR grav 3x3 no OPR
- LAG grav 3x3 + OPR
- LAG+LAR grav 3x3 + OPR for LAG

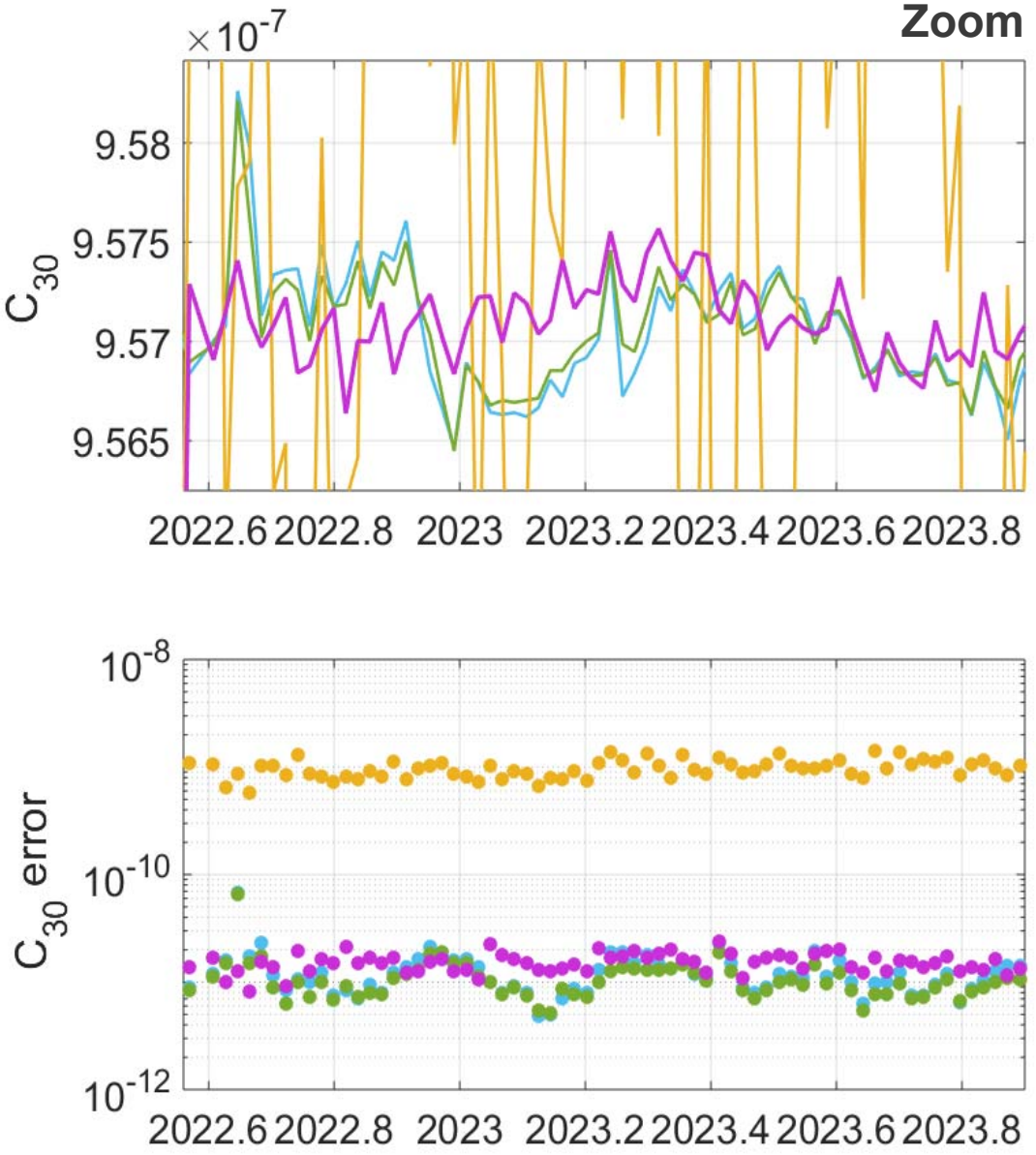

Empirical orbit parameters

LARES-2

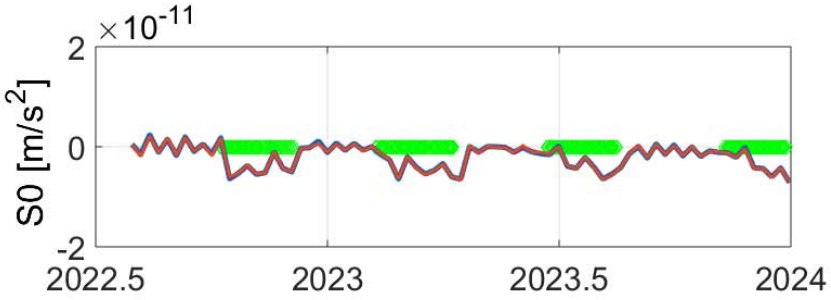

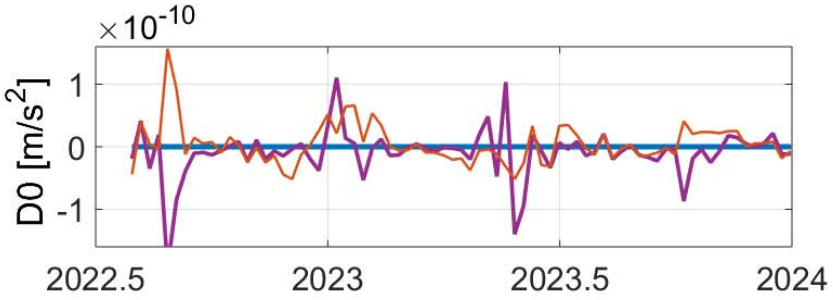

Empirical orbit parameters

LARES-2

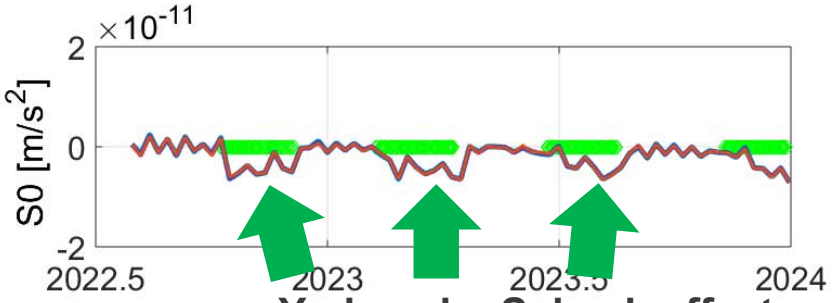

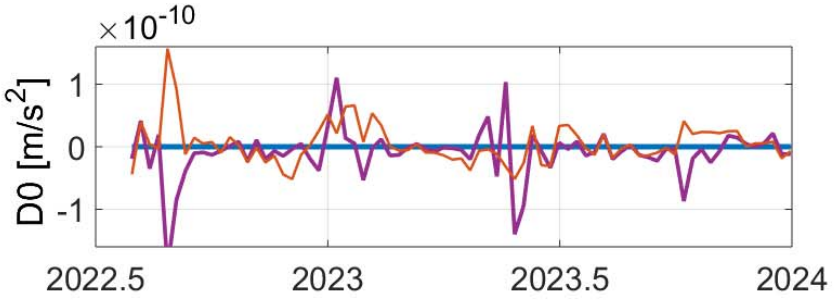

Yarkovsky-Schach effect detectable in eclipsing periods

Empirical orbit parameters

LARES-2

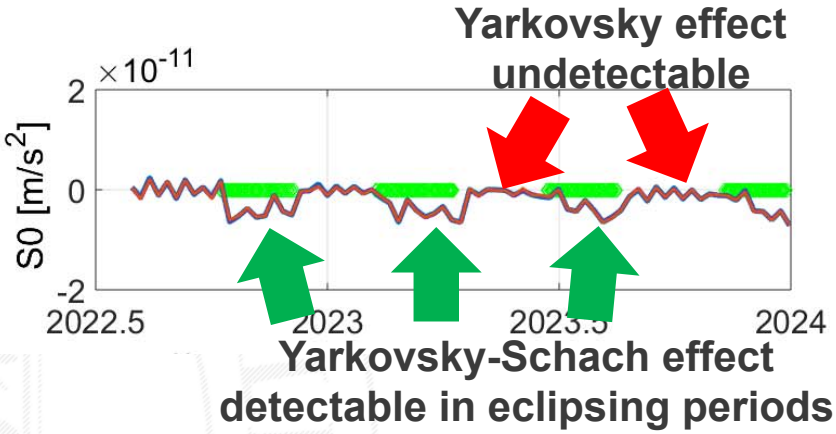

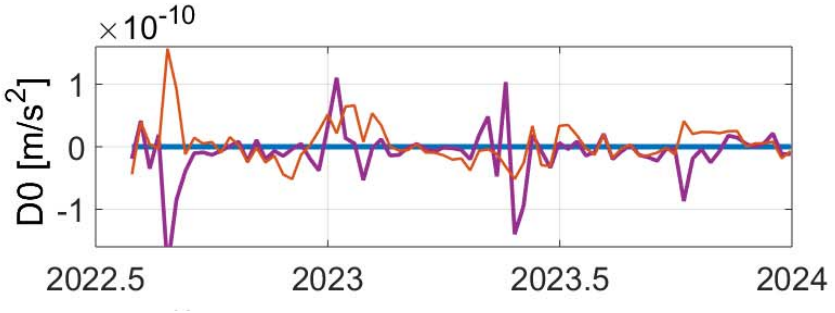

Empirical orbit parameters

LARES-2

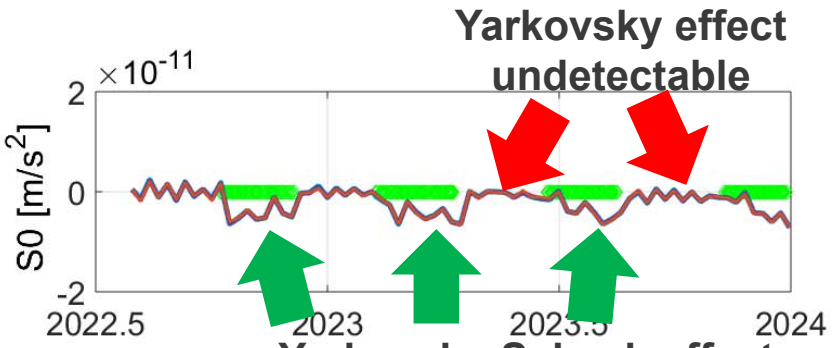

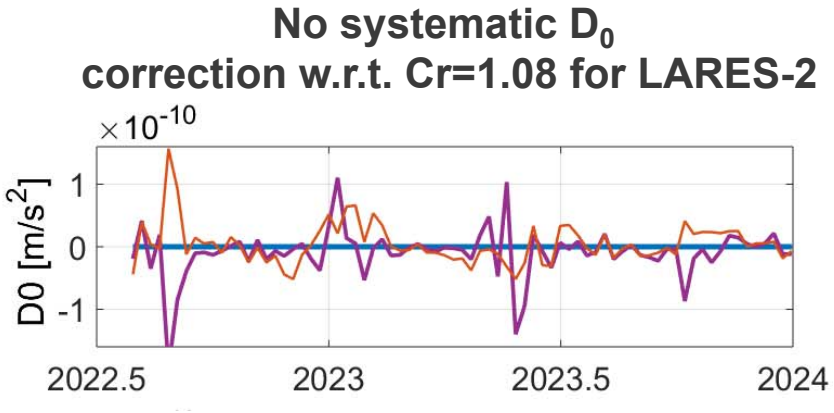

Empirical orbit parameters

LARES-2

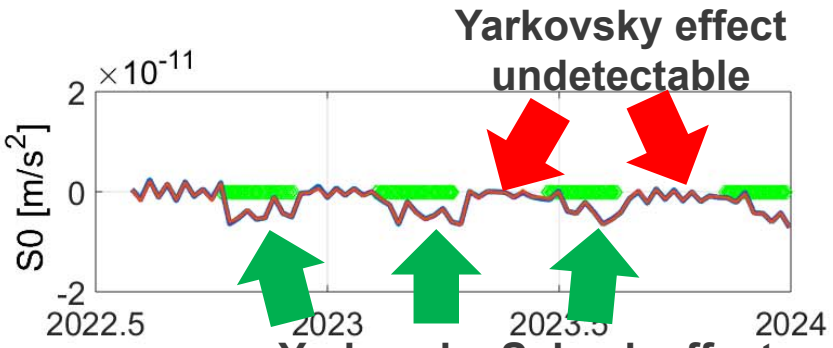

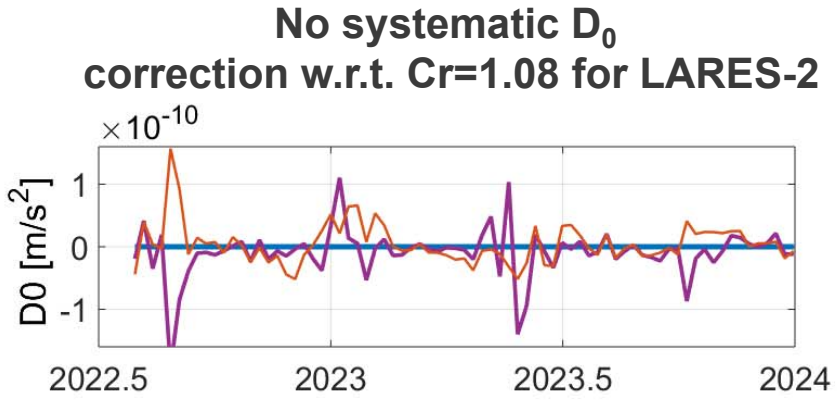

LAGEOS-2

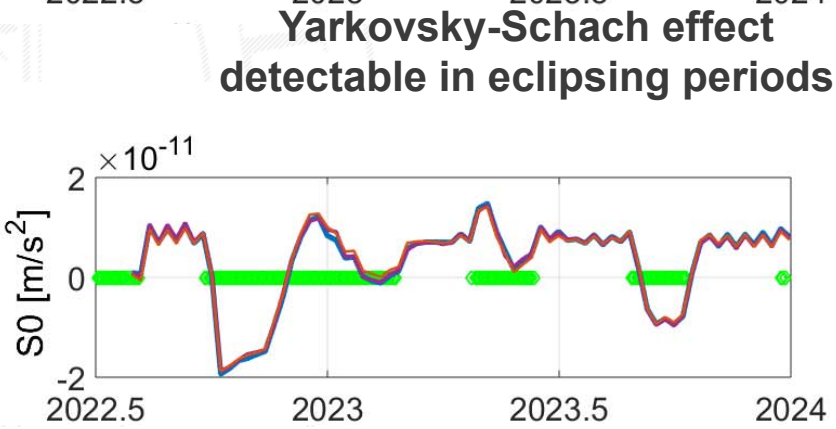

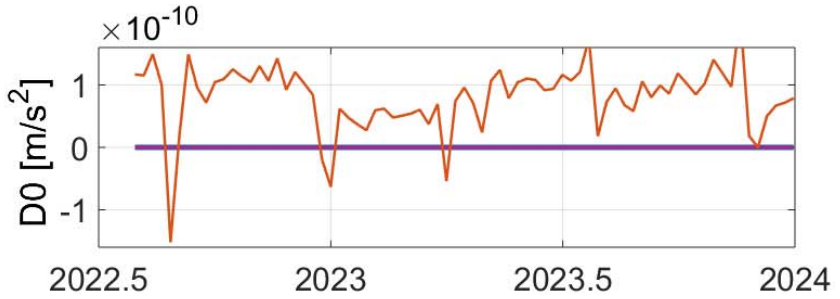

LAGEOS-1

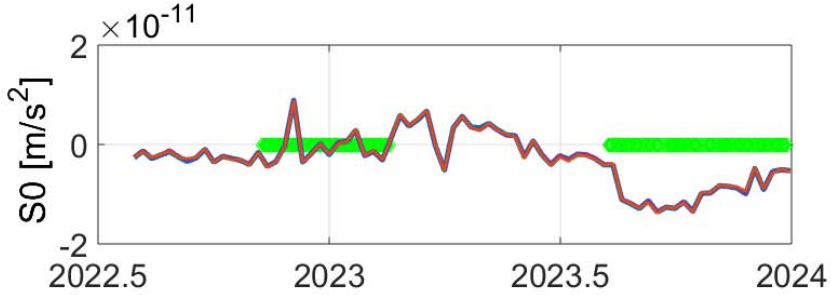

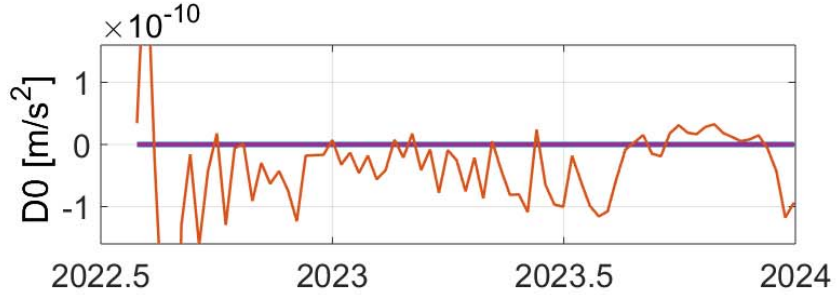

Empirical orbit parameters

LARES-2

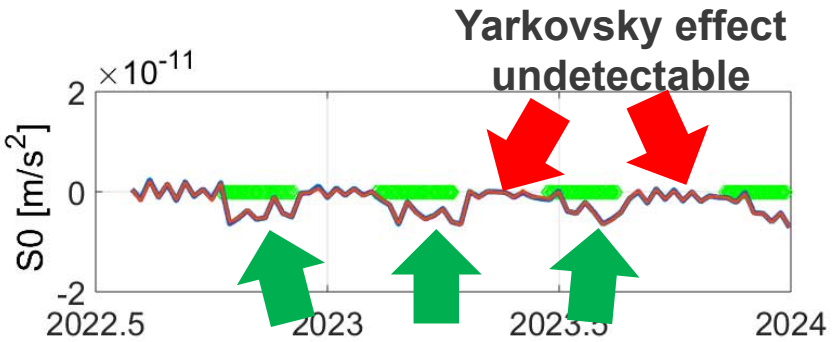

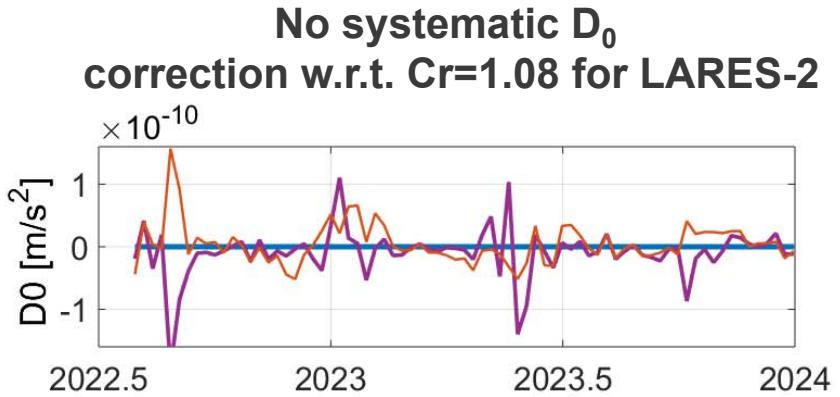

LAGEOS-2

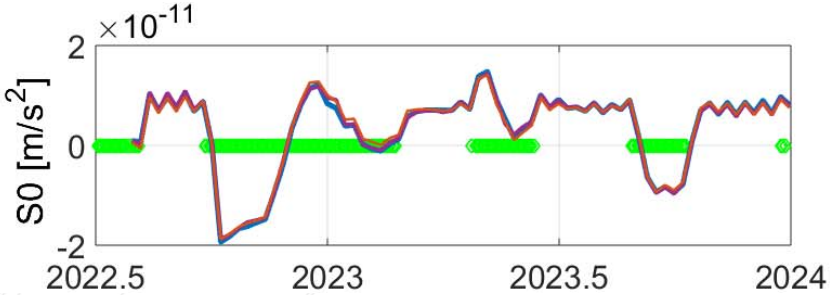

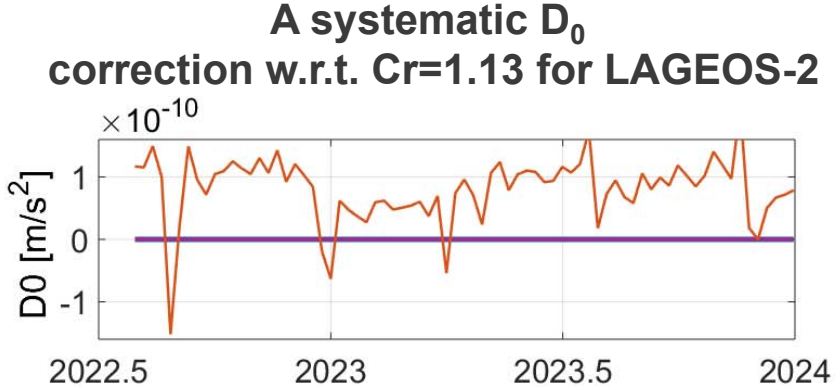

LAGEOS-1

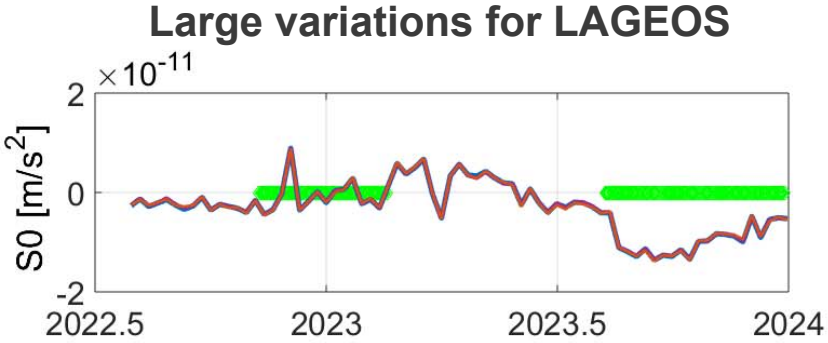

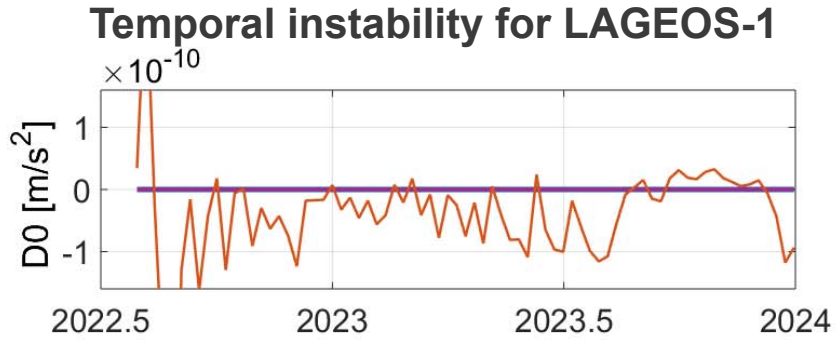

LARES-2 – Earth Rotation Parameters

Adding LARES-2 leads to an improvement in pole coordinate estimates and LOD (a better consistency with the a priori IERS-20-C04 series).

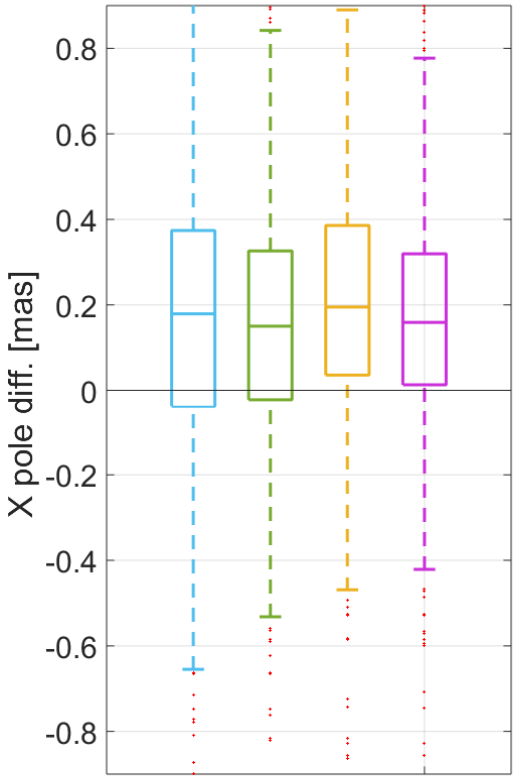

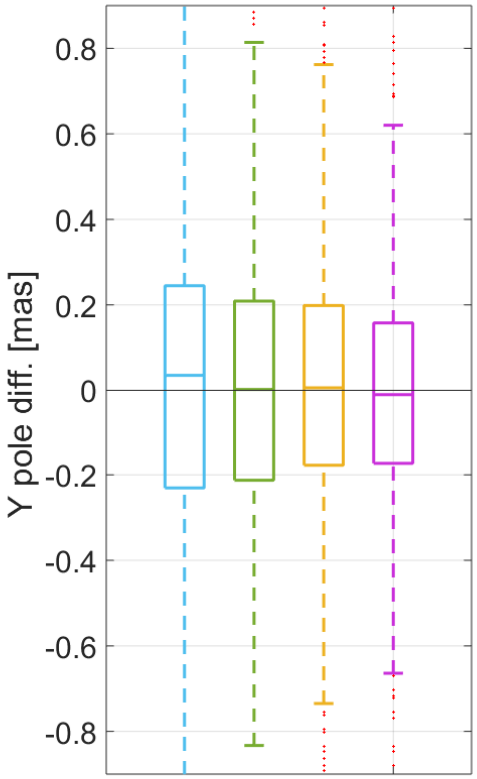

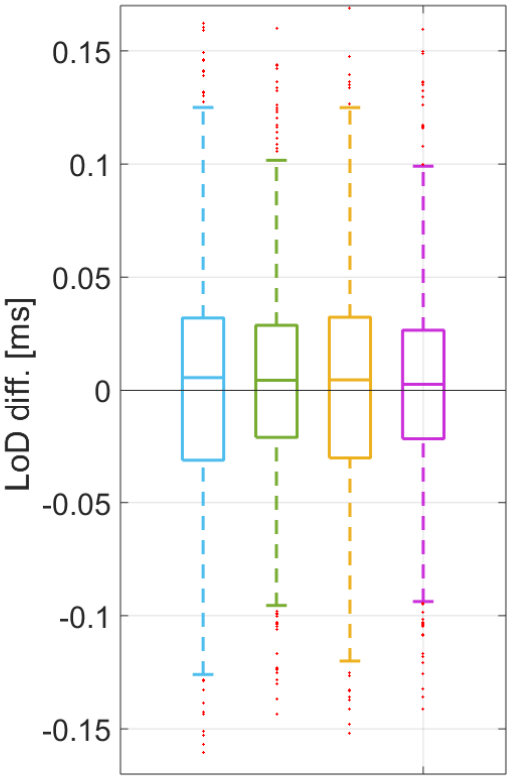

Correlations between C_{20}, C_{30}, Z geocenter and other estimates parameters

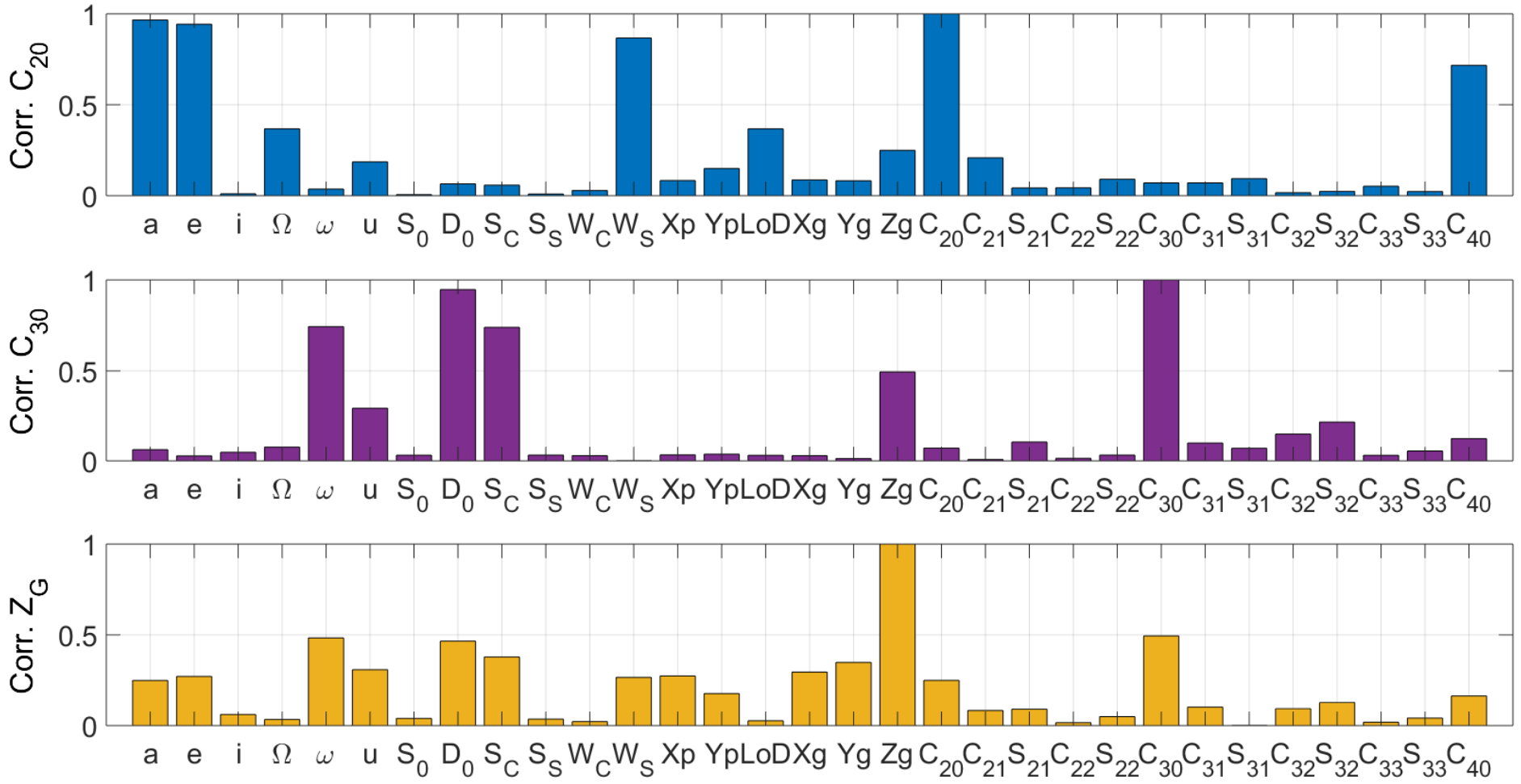

Correlations – Triplet I

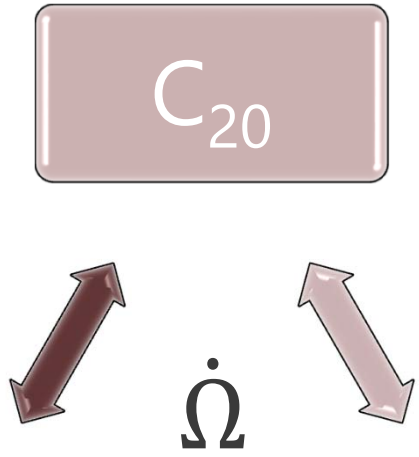

$$\frac{LoD_{mass}}{86400\ s} = \frac{3}{2}\frac{Ma_e^2}{C_M}\Delta C_{20}$$

$$\begin{Bmatrix} R \\ S \\ W \end{Bmatrix} = \frac{3}{2}\frac{GMa_e^2\Delta C_{20}}{r^4}\begin{Bmatrix} 1-\frac{3}{2}\sin^2 i + \frac{3}{2}\sin^2 i \sin^2 u \\ \sin^2 i \sin 2u \\ \sin 2i \sin u \end{Bmatrix}$$

$$\dot{\Omega} = \frac{3}{2}\frac{\sqrt{GM}a_e \cos i}{a^{\frac{7}{2}}(1-e^2)^2}C_{20}$$

$$\frac{LoD}{86400\ s} = (\dot{\Omega} + \dot{u}\cos i)\ \rho^{-1}$$

$$\dot{\Omega} = \frac{r\sin u}{n\ a^2\sqrt{1-e^2}\sin i}W'$$

Correlations – Triplet II

$$V = \frac{GM}{r}\left(1 + \frac{a_e}{r}P_{10}(\cos\theta)C_{10} + \left(\frac{a_e}{r}\right)^2 P_{20}(\cos\theta)C_{20} + \left(\frac{a_e}{r}\right)^3 P_{30}(\cos\theta)C_{30} + \cdots\right)$$

C_{30}

$\dot{e} - i\omega$

Z_G ⟷ D_0/S_c

$$P_{10}(\cos\theta) = \cos\theta$$
$$P_{20}(\cos\theta) = \frac{1}{2}(3\cos^2\theta - 1)$$
$$P_{30}(\cos\theta) = \frac{1}{2}(5\cos^3\theta - 3\cos\theta)$$
$$P_{40}(\cos\theta) = \frac{1}{8}(35\cos^4\theta - 30\cos^2\theta + 3)$$

	P_{10}	P_{20}	P_{30}	P_{40}
P_{10}	1	0.002	0.516	0.003
P_{20}	-	1	0.003	0.498
P_{30}	-	-	1	0.004

$$\begin{Bmatrix} R \\ S \\ W \end{Bmatrix} = D_0 \begin{Bmatrix} \cos\beta\cos\Delta u \\ \cos\beta\sin\Delta u \\ \sin\beta \end{Bmatrix}$$

$$\sin\Delta u = \sin u\cos u_S - \cos u\sin u_S$$

$$\begin{Bmatrix} R \\ S \\ W \end{Bmatrix} = \frac{5}{2}\frac{GMa_e\Delta C_{30}}{r^5} \begin{Bmatrix} \frac{12}{5}\sin i\sin u - 4\sin^3 i\sin^3 u \\ \left(3\sin^3 i\sin^2 u - \frac{3}{5}\sin i\right)\cos u \\ 3\sin^2 i\sin^2 u\cos i - \frac{3}{5}\cos i \end{Bmatrix}$$

$$\begin{Bmatrix} R \\ S \\ W \end{Bmatrix} = \frac{\sqrt{3}}{3}\frac{GM}{r^3}Z_G \begin{Bmatrix} -2\sin i\sin u \\ \sin i\cos u \\ \cos i \end{Bmatrix}$$

$$C_{10} = \sqrt{3}a_e Z_G$$

Empirical orbit parameters OPR in along-track do not allow for C_{30} determination. However, they are needed for LAGEOS-1/2 to absorb Yarkowsky/-Schach effects.

LARES-2 has a different construction (no inner core) and does not have this problem.

Summary

- **LARES-2** orbit is **more stable than LAGEOS-1/2** due to a different satellite construction (**solid sphere**, no inner structure)
- **LARES-2 shows no need for the estimation of D_0**, which is very good news, because it **improves the Z geocenter** component estimation and **C_{30}**. LARES-2 improves Z geocenter by up to 59%.
- **The only empirical parameter that is needed for LARES-2 is S_0** to compensate for the Yarkovsky-Schach effect (whereas the Yarkovsky effect is undetectable)
- The best option for the combined LAGEOS+LARES-2 solution is: grav. field up to 3x3, S_0, S_C, S_S for LAG-1/2 and S_0 for LARES-2
- When emprical orbit parameters OPR in S are not estimated for LAGEOS-1/2, the non-gravitational perturbations affect C_{30} and Z geocenter. However, LARES-2 does not have this problem.

WROCŁAW UNIVERSITY OF ENVIRONMENTAL AND LIFE SCIENCES

Thank you for your attention!

Krzysztof Sośnica
Institute of Geodesy and Geoinformatics, UPWr
krzysztof.sosnica@upwr.edu.pl

LARES-2 – ERPs w.r.t. IERS-C04-20

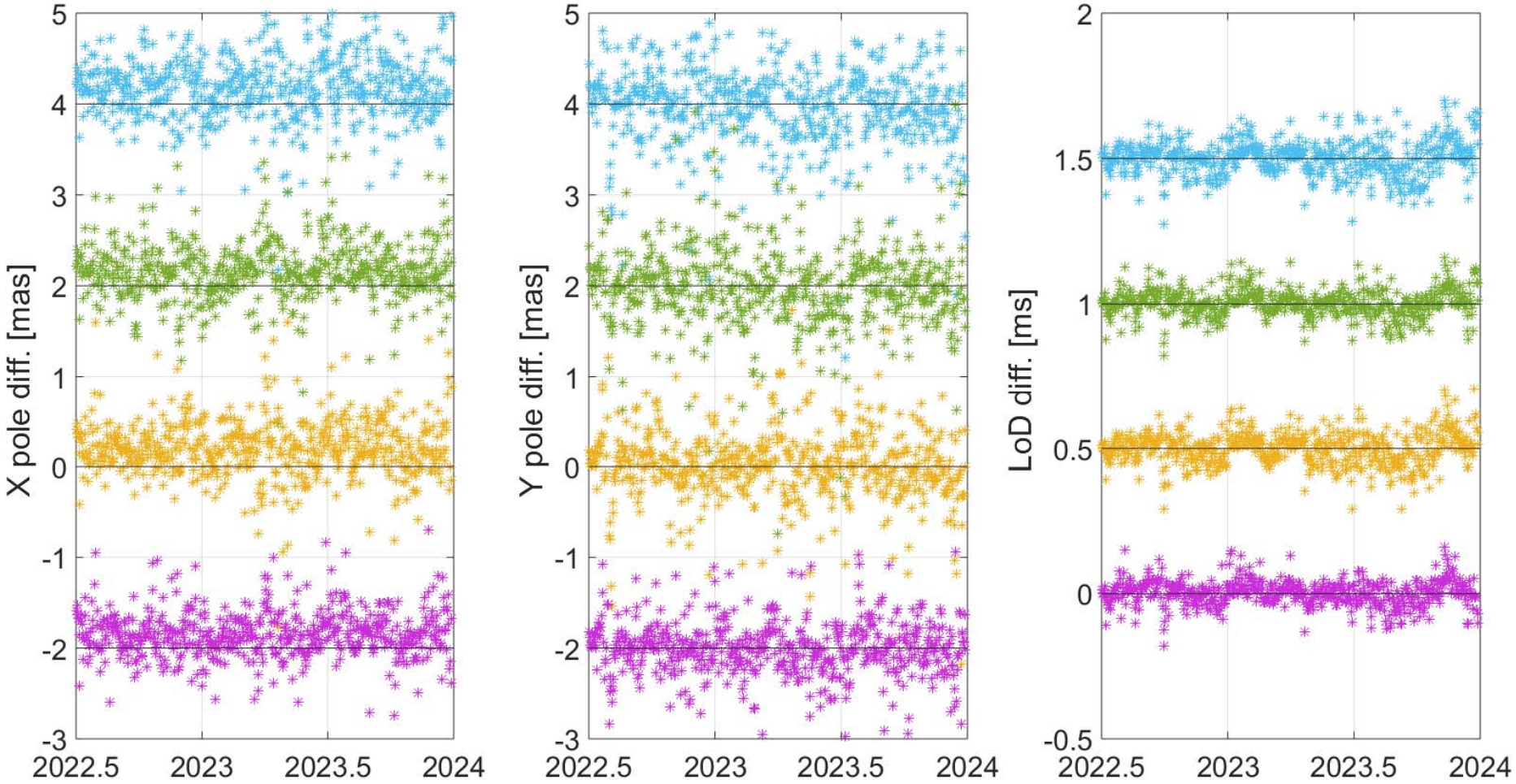

LARES-2

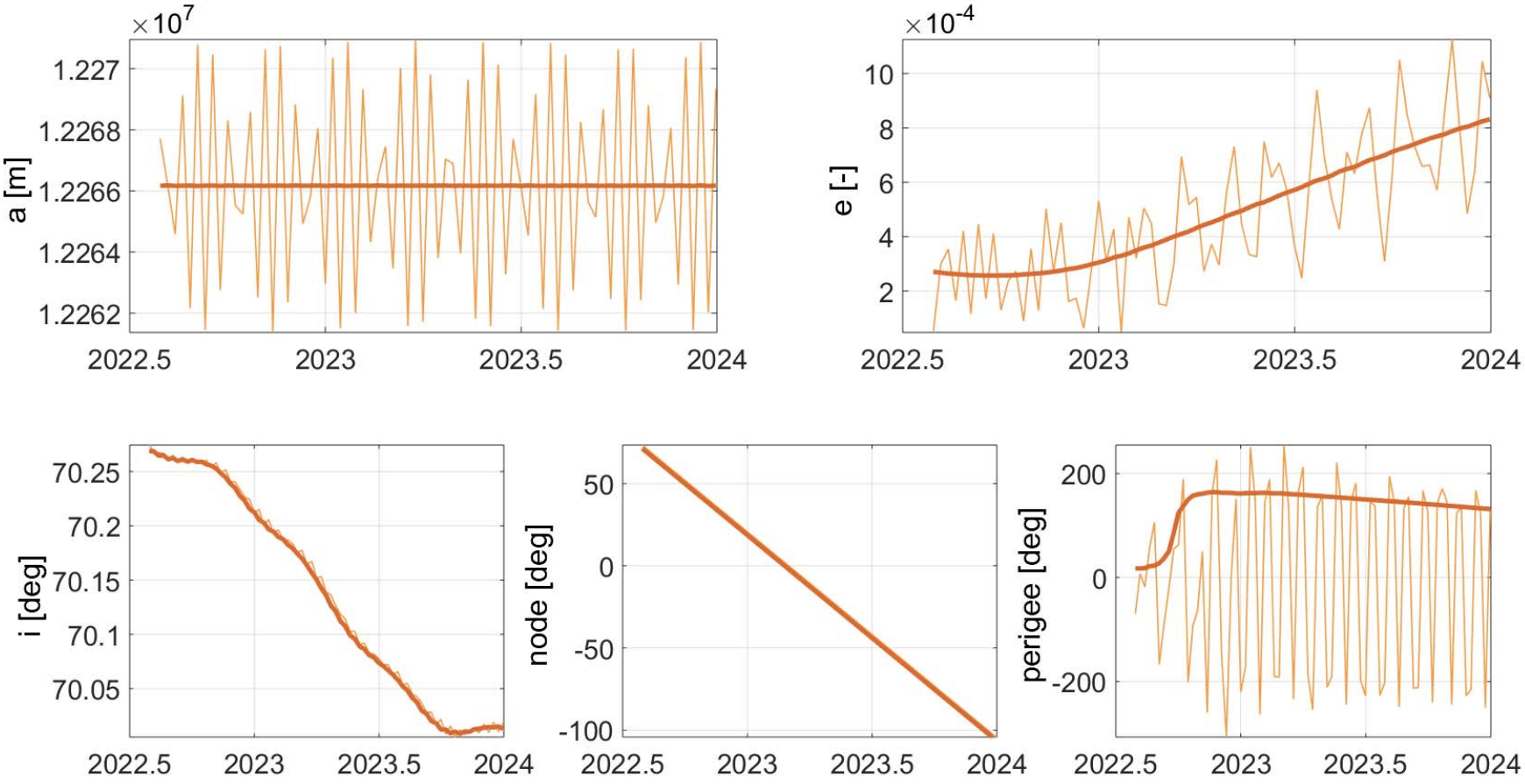

LARES-2 mean and osculating orbital (Keplerian) elements